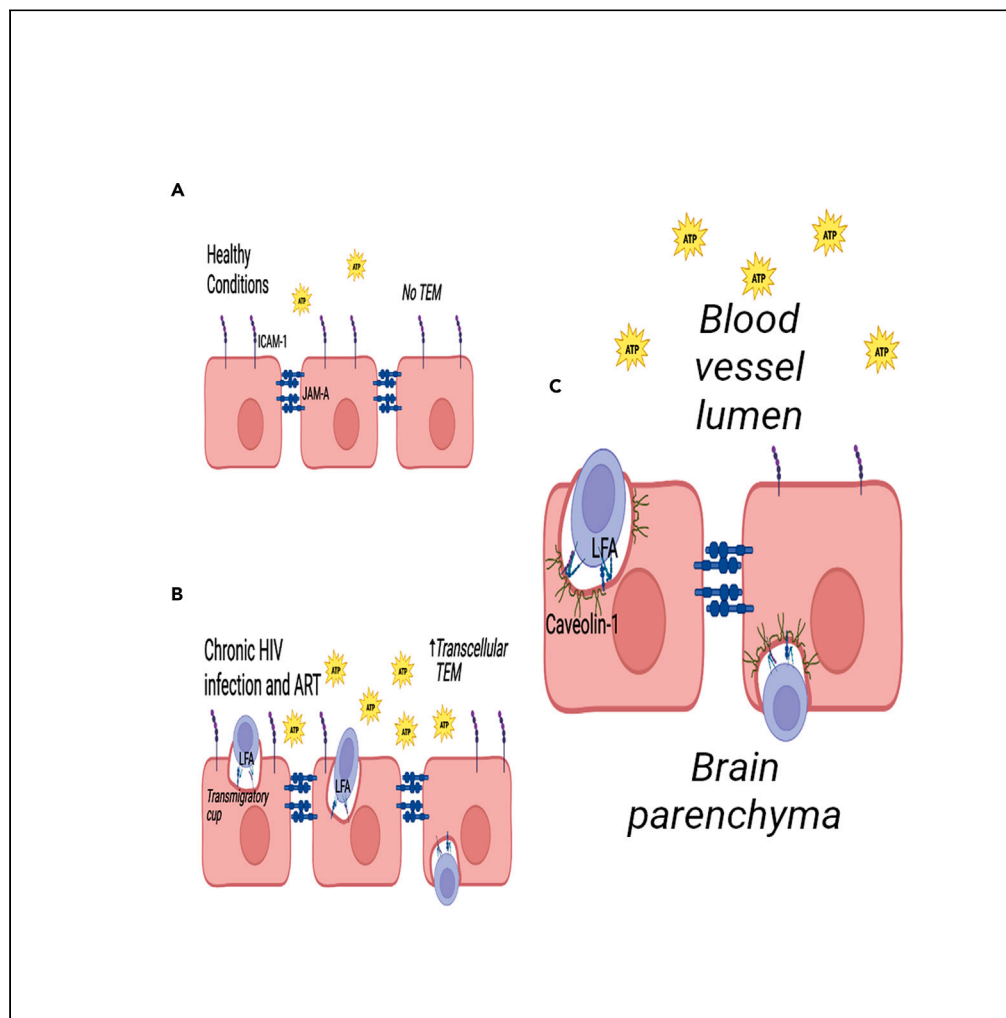


## Article

## Mechanisms of HIV-mediated blood-brain barrier compromise and leukocyte transmigration under the current antiretroviral era



Cristian  
Hernandez, Anna  
Maria Gorska,  
Eliseo Eugenin

eleugeni@utmb.edu

#### Highlights

Serum ATP in PWH and cognitive impairment does not alter the BBB

Serum ATP in PWH and cognitive impairment does not alter leukocyte activation

Serum ATP plus HIV triggers a transcellular leukocyte transmigration

Transcellular transmigration induced by ATP and HIV is LFA-1 and JAM-A dependent

## Article

# Mechanisms of HIV-mediated blood-brain barrier compromise and leukocyte transmigration under the current antiretroviral era

Cristian Hernandez,<sup>1</sup> Anna Maria Gorska,<sup>1,2</sup> and Eliseo Eugenin<sup>1,3,\*</sup>

## SUMMARY

**HIV-associated neurological compromise is observed in more than half of all people with HIV (PWH), even under antiretroviral therapy (ART). The mechanism has been associated with the early transmigration of HIV-infected monocytes across the BBB in a CCL2 and HIV replication-dependent manner. However, the mechanisms of chronic brain damage are unknown.**

**We demonstrate that all PWH under ART have elevated circulating ATP levels that correlate with the onset of cognitive impairment even in the absence of a circulating virus. Serum ATP levels found in PWH with the most severe neurocognitive impairment trigger the transcellular migration of HIV-infected leukocytes across the BBB in a JAM-A and LFA-1-dependent manner. We propose that targeting transcellular leukocyte transmigration could reduce or prevent the devastating consequences of HIV within the brains of PWH under ART.**

## INTRODUCTION

Currently, there are about 38.5 million people with HIV (PWH) worldwide, with an estimated 15–50% of those living with HIV-associated neurocognitive disorder (HAND).<sup>1,2</sup> HAND is a spectrum of neurocognitive disorders that vary in severity from asymptomatic neurocognitive impairment (ANI) to mild neurocognitive disorder (MND) to HIV-associated dementia (HAD), the most severe.<sup>1</sup> Clinical monitoring of HANDs uses a regular (three-to-six-month interval) battery of cognitive tests involving six criteria: language, memory, attention, motor function, executive functions, and processing speed.<sup>3</sup> Biomarkers from either serum or cerebral spinal fluid (CSF), are available for screening and diagnosis for HIV-associated dementia; however, there are currently no identifiable biomarkers for less severe HANDs.<sup>4–6</sup> Our laboratory demonstrated that adenosine triphosphate (ATP) concentration within serum correlates with neurocognitive impairment in PWH.<sup>7</sup> However, the mechanisms by which extracellular ATP (eATP) relates to cognitive impairment in the PWH are unknown.

Our published data demonstrated that eATP, Pannexin-1 channels (Pax-1), and the purinergic receptor axis are essential for the initial steps of HIV infection and replication by a mechanism involving the purinergic receptors P2X<sub>1</sub>, X<sub>7</sub>, and Y<sub>1</sub>.<sup>8,9</sup> Pax-1 forms hemichannels at the plasma membrane and are typically constitutively closed in non-pathological conditions. However, during pathological conditions or certain cell functions such as chemokine signaling, T cell differentiation, and apoptosis, the Pax-1 channel opens and releases cytoplasmic inflammatory molecules such as ATP, which signals through purinergic receptors.<sup>10</sup> Pax-1 inhibition prevents synaptic and neuronal compromise within the brains of SIV-infected macaques, demonstrating that Pax-1 opening plays a critical role in HAND pathogenesis.<sup>11</sup> However, all these data were obtained during acute infection; thus, how eATP in chronic conditions can predict or contribute to cognitive impairment is unknown. Normally, eATP is degraded quickly (on the order of seconds to minutes) by ectoATPases to prevent the overactivation of purinergic receptors.<sup>12,13</sup> Within the serum of aviremic PWH, the concentration of ATP is stable and is persistently released by Pax-1 channels of circulating leukocytes and likely by other cell types.<sup>7</sup>

In physiological and pathological conditions, including HIV infection, transendothelial migration (TEM) is a key mechanism for viral tissue invasion, the formation of viral reservoirs, and immune patrolling.<sup>12</sup> In physiological conditions, upon inflammatory stimuli, leukocytes show activation, arresting, rolling, adhesion, and locomotion onto and through the endothelium.<sup>14</sup> Most of these cell-to-cell interactions are weak and reversible. Then, leukocytes commit to diapedesis, and the best-described mechanism of transmigration is by a paracellular route between two or more adjacent endothelial cells.<sup>14</sup> Instead, neutrophils can use a different mechanism, transcellular migration, through the endothelial cell body.<sup>15</sup> Paracellular migration is highly coordinated between the endothelium and leukocyte to compete and secrete metalloproteases to coordinate a controlled opening of the endothelium junctions to enable the leukocyte to cross them.<sup>16</sup> The molecules

<sup>1</sup>Department of Neurobiology, The University of Texas Medical Branch (UTMB), Galveston, TX, USA

<sup>2</sup>Department of Pathology, University of Oslo, Oslo, Norway

<sup>3</sup>Lead contact

\*Correspondence: [eleugini@utmb.edu](mailto:eleugini@utmb.edu)

<https://doi.org/10.1016/j.isci.2024.109236>



involved in these leukocyte-endothelial or endothelial-endothelial interactions are occludin, zona occludens (ZO-1), claudins, junction adhesion molecules (JAMs), intercellular adhesion molecules (ICAM-1), vascular cell adhesion molecule (VCAM-1), CD99, platelet and endothelial cell adhesion molecule (PECAM-1), lymphocyte function-associated antigen 1 (LFA-1), and very late antigen 4 (VLA-4).<sup>14</sup> Dr. Berman's lab demonstrated that paracellular transmigration is the primary means by which HIV-infected leukocytes, including a subset of monocytes (CD14<sup>+</sup>CD16<sup>+</sup>), infiltrate the brain during acute infection.<sup>17–19</sup> In contrast, transcellular is less characterized, involving VCAM-1, ICAM-1, caveolin-1, vinculin, Wiskott-Aldrich syndrome protein (WASP), and LFA-1, with the formation of a specialized cellular cup to enable transmigration across the endothelial cytoplasm.<sup>20</sup> However, whether these mechanisms are present during chronic HIV infection is not fully understood.

We demonstrated that chronic HIV infection resulted in high levels of eATP in the serum correlating with cognitive impairment.<sup>7</sup> Increased eATP minimally compromised the expression and localization of cell adhesion molecules (CAMs) and tight junction proteins on brain microvascular endothelial cells and leukocytes but triggered the transcellular transmigration of mostly HIV-infected leukocytes across the blood-brain barrier (BBB). Transcellular migration induced by HIV infection and high eATP was JAM-A and LFA-1 dependent. We believe that preventing leukocyte brain invasion induced by high eATP and HIV could reduce cognitive impairment observed within PWH under ART.

## RESULTS

### Extracellular adenosine triphosphate concentrations identified in uninfected and human immunodeficiency virus infected people with associated dementia do not compromise brain microvascular endothelial or leukocyte survival

Overactivation of purinergic receptors by eATP generally results in inflammation and apoptosis.<sup>21</sup> A full screening of the profile of the purinergic system in primary human BMVEC by quantitative reverse transcriptase polymerase chain reaction (qRT-PCR; primer sequences in Table S1) and Western blot analysis of primary BMVEC indicated a lack or low expression of large ionic purinergic channels associated with inflammation and apoptosis, such as P2X<sub>7</sub> (Figure S1A). BMVEC expressed P2Y<sub>1</sub>, P2Y<sub>2</sub>, P2Y<sub>4</sub>, P2Y<sub>5</sub>, P2Y<sub>6</sub>, P2Y<sub>8</sub> (Figure S1A), ecto 5'-nucleotidase (NT5E or CD73) (Figure S1B), and adenosine (ado) receptor A<sub>2B</sub> as the major purinergic components as analyzed by qRT-PCR (Figure S1C). Western blot analysis of BMVEC cultures at low (less than 7) and high (8–13 passages) passages did not show changes in protein expression for the P2X, P2Y, and eATP metabolism enzymes (Figures S1D and S1E). O<sup>6</sup>-methylguanine-DNA-methyltransferase (MGMT) was used as a negative control and PECAM-1 as a positive control for amplification (Figures S1A–S1C). Overall, no significant changes in mRNA or protein expression in the purinergic system were detected among different donors' BMVEC, thus, the purinergic profile was consistent (n = 4, from different donors).

Based on the purinergic receptor screening results, primary BMVEC of different donors express purinergic P2 receptor (P2X and P2Y), one adenosinergic P1 receptor (A<sub>2B</sub>), eATP metabolism enzymes including nucleotide pyrophosphatase/phosphodiesterase (NPP1, NPP2, and NPP3), ectonucleotidases (NTPDase1, NTPDase2, NTPDase3, and NTPDase5; members of the CD39 family, also referred to as ENTPD enzymes), NT5E/CD73, adenosine deaminase (ADA), and alkaline phosphatase (ALP). Normally, eATP is degraded in seconds-minutes,<sup>12</sup> thus, we mimicked the eATP stability observed in the serum of PWH using ATP $\gamma$ S due to its pharmacological properties on non-P2X<sub>4/7</sub> receptors, including those expressed by BMVEC, as well as its increased stability to ectonucleotidases.<sup>12,22–24</sup>

Chronic (up to 7 passages or 35+ days) treatment of BMVEC or PBMCs with ATP $\gamma$ S concentrations, 3  $\mu$ M (uninfected individuals) or 15  $\mu$ M (eATP concentration associated with HAD in serum of PWH), did not change PBMC viability (n = 3, untreated: 87  $\pm$  10%, 3  $\mu$ M: 86  $\pm$  8%, 15  $\mu$ M: 89  $\pm$  6%, HIV:89  $\pm$  3%, 3  $\mu$ M + HIV: 85  $\pm$  5%, 15  $\mu$ M + HIV: 85  $\pm$  4%) or BMVEC proliferation (n = 3, n.s., p = 0.056 by linear regression, untreated slope: 0.588, 3  $\mu$ M slope: 0.674, 15  $\mu$ M slope: 0.773) in the presence or absence of HIV infection of PBMCs (Figures S2A and S2B). Thus, ATP $\gamma$ S treatment, 3 or 15  $\mu$ M, is not toxic in PBMC or BMVEC. We chose for the following experiments, media as control (media containing 1.9  $\pm$  1.3  $\mu$ M of hydrolyzable ATP), healthy ATP levels 3  $\mu$ M that correspond to the high end (range of ATP in healthy people 1–3  $\mu$ M, including with comorbidities), and lastly, 15  $\mu$ M ATP $\gamma$ S that correspond to the ATP levels present in the serum of PWH and HAD.<sup>7</sup> Also, the concentrations were selected based on the maximal serum level present in healthy non-infected individuals and PWH with dementia, respectively.

### Extracellular adenosine triphosphate described in people with human immunodeficiency virus and associated dementia did not change the expression and distribution of key adhesion and tight junction proteins as well as extracellular adenosine triphosphate metabolism enzymes on brain microvascular endothelial cells

An integral function of the BBB is to exclude leukocytes from the brain, but during inflammation, leukocytes transmigrate in a controlled manner using highly specialized heterophilic and homophilic interactions between cell adhesion molecules and integrins between leukocytes and activated endothelial cells (EC).<sup>14,25</sup> Our published data during acute HIV infection demonstrated that brain HIV invasion and BBB disruption are dependent on viral replication and CCL2,<sup>17,26</sup> but the mechanisms of brain compromise during chronic infection are unknown.

First, we examine the effects of ATP on BMVEC (ATP $\gamma$ S, 3 and 15  $\mu$ M). BMVEC treated with 3  $\mu$ M (physiological concentration) or 15  $\mu$ M (HAD-associated eATP concentration) ATP $\gamma$ S were examined for the expression of tight junction (occludin, ZO-1, and claudin-1), adhesion molecules (ICAM-1 and platelet and endothelial cell adhesion molecule, PECAM-1), junctional proteins (JAM-A, -B, -C, and CD99), and eATP metabolism enzymes (ENTPD-1/CD39; NT5E/CD73; and adenosine/ado deaminase) by Western blot and FACS (Figures 1 and S3D–S3F). Western blot analyses indicated no significant change in all described proteins comparing untreated, 3  $\mu$ M, and 15  $\mu$ M ATP $\gamma$ S treatments (Figures 1A–1D and quantification in E, n = 3–7 independent experiments, representative Western blot images shown). However,

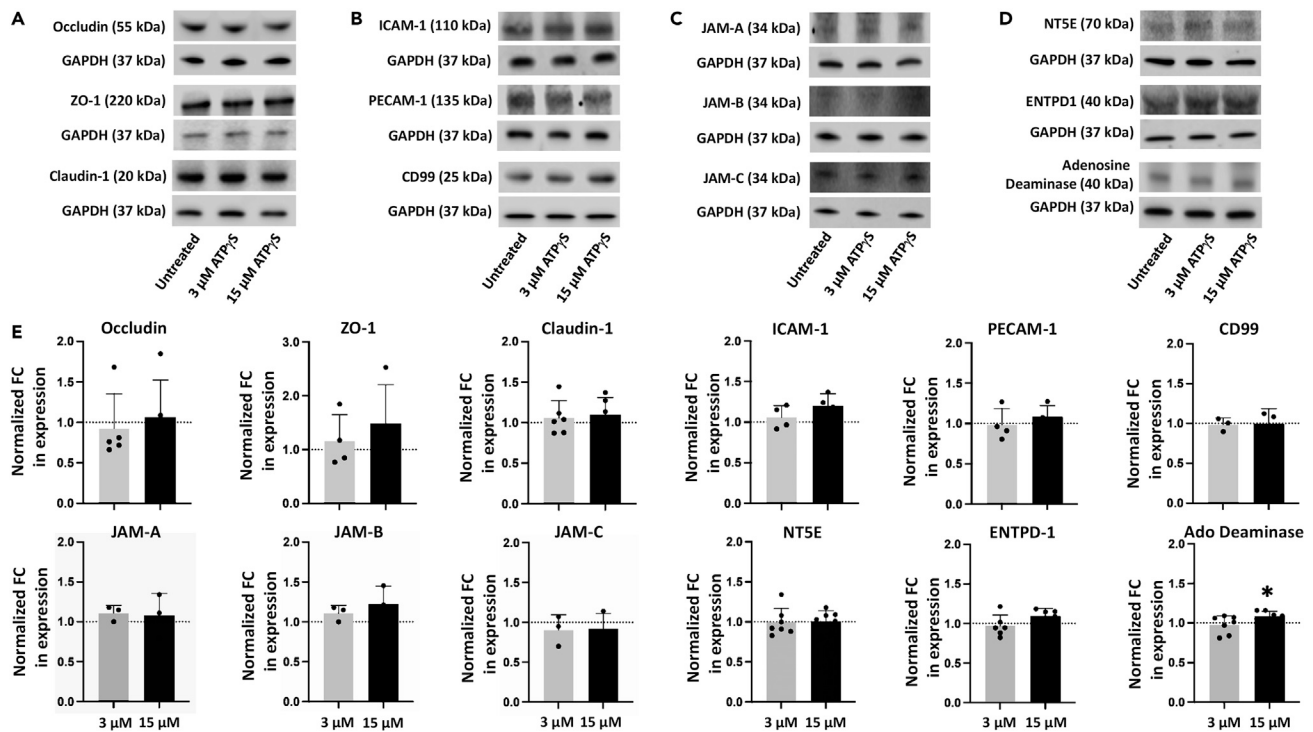


**Figure 1. Cell adhesion, junctional, and eATP metabolism enzymes expressed by primary human brain microvascular endothelial cells (BMVEC) are not altered by treatment with ATP $\gamma$ S**

BMVEC were grown to confluence in the presence of 3 or 15  $\mu$ M of ATP $\gamma$ S (for a single passage or multiple passages), and whole cell lysate was subjected to Western blot.

(A) Representative blots for occludin, ZO-1, and claudin-1; (B) ICAM-1, PECAM-1, CD99; (C) JAM-A, -B, and -C, and (D) NT5E/CD73, ENTPD1/CD39, and adenosine (ado) deaminase in untreated, 3  $\mu$ M and 15  $\mu$ M ATP $\gamma$ S. GAPDH was used as a loading control (representative western blots are shown).

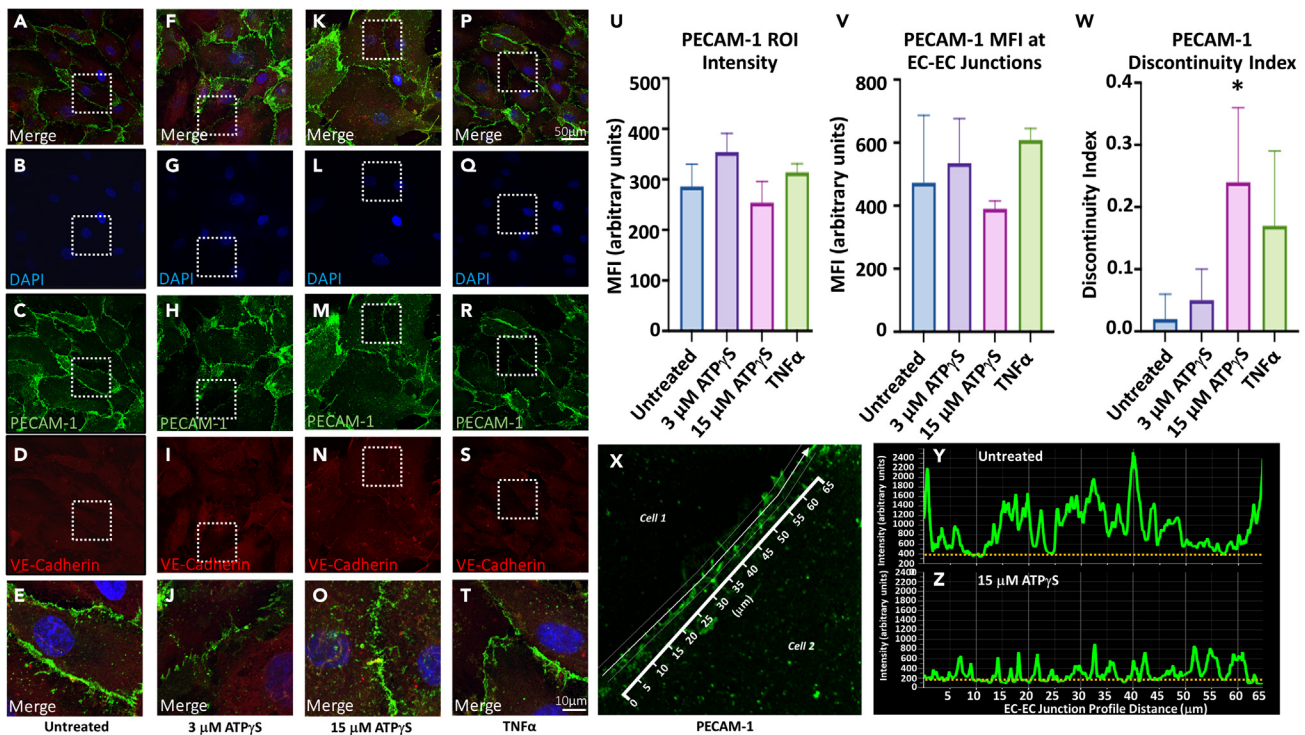
(E) correspond to the quantification of the Western blot data calibrated to untreated conditions,  $n = 3-7$  independent experiments. Densitometric analysis was conducted using the target intensity, normalized to the loading control, represented as a fold change compared to corresponding untreated; gray bars represent 3  $\mu$ M and black bars represent 15  $\mu$ M. Only adenosine deaminase was upregulated in 15  $\mu$ M ATP treatment ( $n = 7$ ,  $*p < 0.0122$ ,  $1.08 \pm 0.063$ -fold change), compared to untreated. Data are represented as mean  $\pm$  standard deviation. Significance was determined using Wilcoxon Signed Rank test.  $*p < 0.05$ .

among the proteins involved in eATP metabolism, adenosine deaminase was significantly increased in the 15  $\mu$ M condition,  $1.08 \pm 0.063$  fold-change (Figures 1D and 1E,  $n = 7$ ,  $*p < 0.0122$  compared to the untreated condition). As denoted in Figures S3A–S3C, the process of attachment and transmigration as well as BBB permeability are controlled by specific adhesion and junctional interactions.<sup>27</sup> Thus, we examined whether ATP $\gamma$ S (3  $\mu$ M or 15  $\mu$ M) alters the surface distribution of adhesion molecules (ICAM-1), junctional proteins (JAM-A and CD99), and an eATP metabolism enzyme (NT5E/CD73) by flow cytometry in BMVEC. Overall, there were no significant changes in the surface distribution of the surface proteins analyzed in ATP $\gamma$ S-treated BMVEC (Figures S3D–S3F).

A critical hallmark of HAD in viremic patients is the shedding of PECAM-1 at the plasma membrane and its accumulation at the BBB with significant leukocyte transmigration to the brain,<sup>28</sup> but whether this occurs within chronic conditions is unknown. We examined whether PECAM-1 was shed upon ATP $\gamma$ S treatment by quantifying total PECAM-1 (Figures 1E and S4A), and the  $\sim 20$  kDa cleaved PECAM-1 (cPECAM-1) fragment (Figures S4B and S4C). Our data during acute HIV infection also denote a key role of P2Y<sub>1</sub> and MMP-2, however, both were not affected by ATP $\gamma$ S treatment (see Figures S4B and S4C). We also increased the treatment duration of BMVEC to ATP $\gamma$ S to multiple passages (up to 7–8 passages), referred to as chronic treatment. Despite the increased ATP $\gamma$ S treatment duration, no significant changes in PECAM-1 or ZO-1 protein expression by Western blot were observed (Figure S4A,  $n = 3$ ). Overall, our data indicates that chronic brain damage in PWH and associated with high eATP did not change the expression of key adhesion and junctional proteins altered during acute infection, suggesting a different mechanism.

### Extracellular adenosine triphosphate concentrations identified in people with human immunodeficiency virus and associated dementia disrupt platelet and endothelial cell adhesion molecule-1 localization in brain microvascular endothelial cells

To characterize whether physiological (3  $\mu$ M) or HAD-associated (15  $\mu$ M) eATP concentrations alter the distribution of adhesion and junctional proteins in BMVEC as described in Figure 1, we analyzed the expression and distribution of tight junction and cell adhesion



molecules by immunofluorescence, confocal microscopy, image reconstruction, and quantification as described within the STAR Methods section. Representative images of untreated BMVEC (Figures 2A–2E), or treatment with 3  $\mu$ M ATP $\gamma$ S (Figures 2F–2J), 15  $\mu$ M ATP $\gamma$ S (Figures 2K–2O), or TNF $\alpha$  (Figures 2P–2T) show the cellular distribution of PECAM-1. We focused on total intensity, junctional intensity, and a calculated discontinuity index staining at the cellular junctions (Figure 2). Overall, no changes in intracellular or cell junction distribution were detected for occludin, ZO-1, claudin-1, ICAM-1, CD99, JAM-B, and JAM-C for all three parameters (data not shown). However, the imaging analysis identified two proteins with altered localization in response to HAD-associated eATP concentration - PECAM-1 (Figure 2) and JAM-A (Figure 3). In untreated conditions, PECAM-1 (Figures 2A–2E) surrounded the cells in perfect colocalization with VE-Cadherin, a major determinant of endothelial contact integrity at the EC-EC junctions.<sup>29</sup> Among the three treatment conditions, there was no significant change in mean fluorescence intensity (MFI) of PECAM-1 (Figure 2U, n = 3), in agreement with the Western blot results. As far as PECAM-1 intensity at the EC-EC junctions, there was no significant change in MFI among the 3, 15  $\mu$ M ATP $\gamma$ S, and TNF $\alpha$  conditions, compared to untreated conditions (Figure 2V, n = 3). To quantitate the discontinuity of PECAM-1 localized at the EC-EC junctions, we used a thresholding calculation method, referred to as the discontinuity index (detailed within STAR Methods). Per this analysis, PECAM-1 distribution among the EC-EC junctions was disrupted within only the 15  $\mu$ M ATP $\gamma$ S condition (Figure 2W, n = 3, \*p < 0.05, discontinuity indices of 0.26  $\pm$  0.05 and 0.08  $\pm$  0.05 for 15  $\mu$ M and untreated, respectively), suggesting that there are more gaps in PECAM-1 localization to EC-EC junctions. Figure 2X shows a representative example of the quantitation of PECAM-1 localization between two cells and Figures 2Y and 2Z demonstrate the PECAM-1 intensity along the EC-EC junction was below the threshold for 15  $\mu$ M ATP $\gamma$ S, suggesting greater discontinuity, relative to untreated. Overall, HAD-associated eATP compromised PECAM-1 distribution between two or

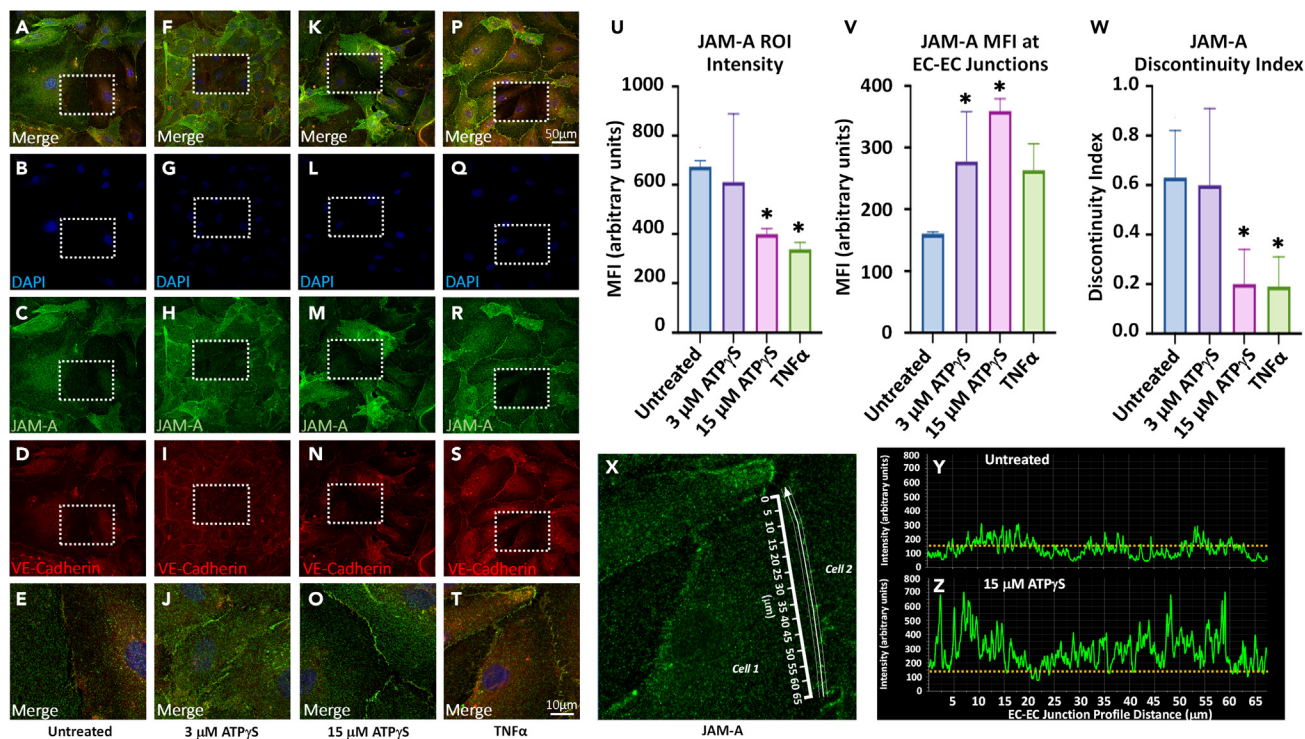


### Figure 3. JAM-A localization at EC-EC junctions is increased by acute HAD-associated eATP treatment

Despite that JAM-A protein levels and surface distribution were not affected by ATPγS treatment (see Figure 1), we determined that 15 μM ATPγS treatment changed its distribution at the EC-EC junctions using confocal microscopy and image analysis than for PECAM-1 (see Figure 2).

(A–E) Representative images of untreated BMVEC stained for DAPI (nuclei, blue staining), JAM-A (green staining), and VE-cadherin (red staining). Merge is the reconstruction of all colors. (E, J, O, T) contain an inset of the white box within the merge.

(F–J) Staining for BMVEC acutely treated with 3 μM ATPγS and (K–O) corresponds to 15 μM ATPγS treatment.

(P–T) TNFα was used as a positive control.

(U) Image quantification of a representative experiment, MFI of JAM-A within full field ROIs (Figure 3U,  $n = 3$ ,  $*p < 0.0005$  with an MFI of  $399 \pm 22$  and  $338 \pm 27$  for 15 μM ATPγS and TNFα, respectively; an MFI of  $674 \pm 25$  for untreated).

(V) Quantification of JAM-A intensity at the EC-EC cell junctions ( $n = 3$ ,  $*p < 0.05$ , an MFI of  $277 \pm 81$  and  $359 \pm 20$  for 3 μM and 15 μM, respectively; an MFI of  $160 \pm 3$  for untreated).

(W) JAM-A discontinuity index calculated by continuous expression at EC-EC junctions ( $n = 3$ ,  $*p < 0.0005$ , a discontinuity index of  $0.20 \pm 0.14$  and  $0.63 \pm 0.19$  for 15 μM ATPγS and untreated, respectively; TNFα had a discontinuity index of  $0.19 \pm 0.12$ ).

(X) corresponds to an image of how the discontinuity index along an EC-EC junction was derived and the increased JAM-A localization to the EC junctions.

(Y) corresponds to the EC junction intensity of JAM-A of untreated and (Z) corresponds to the EC-EC junction intensity of 15 μM ATPγS (yellow bar corresponds to the threshold used, derived from JAM-A intensity within the cell). Data are represented as mean  $\pm$  standard deviation. Significance was determined using Wilcoxon Signed Rank test.  $*p \leq 0.05$ .

more endothelial cells, but not other adhesion of junctional proteins, suggesting a mild effect on BBB function even at a high ATP concentration, 15 μM.

### Junction adhesion molecules-A distribution within brain microvascular endothelial cells is compromised by extracellular adenosine triphosphate concentrations identified in the serum of people with human immunodeficiency virus and associated dementia

BMVECs were grown to confluence in the absence or presence of 3 μM or 15 μM ATPγS and the analysis described for PECAM-1 was performed for JAM-A. In untreated conditions, JAM-A was largely localized to the cytoplasm with little colocalizing with VE-cadherin at the EC-EC junctions (Figures 3A–3E). Representative images of BMVEC treated with 3 μM ATPγS (Figures 3F–3J), 15 μM ATPγS (Figures 3K–3O), or TNFα (Figures 3P–3T) identified an increase in JAM-A localization to EC-EC junctions. Quantification of total JAM-A intensity showed a decrease in total JAM-A expression within both the 15 μM ATPγS and TNFα conditions, compared to untreated (Figure 3U,  $n = 3$ ,  $*p < 0.0005$  with an MFI of  $399 \pm 22$  and  $338 \pm 27$  for 15 μM ATPγS and TNFα, respectively; an MFI of  $674 \pm 25$  for untreated). JAM-A intensity at EC-EC junctions significantly increased for both the 3 μM and 15 μM ATPγS conditions, compared to untreated (Figure 3V,  $n = 3$ ,  $*p < 0.05$ , an MFI of  $277 \pm 81$  and  $359 \pm 20$  for 3 μM and 15 μM, respectively; an MFI of  $160 \pm 3$  for untreated). As far as the discontinuity index, both untreated and 3 μM ATPγS had little JAM-A localization at an intensity higher than the cellular

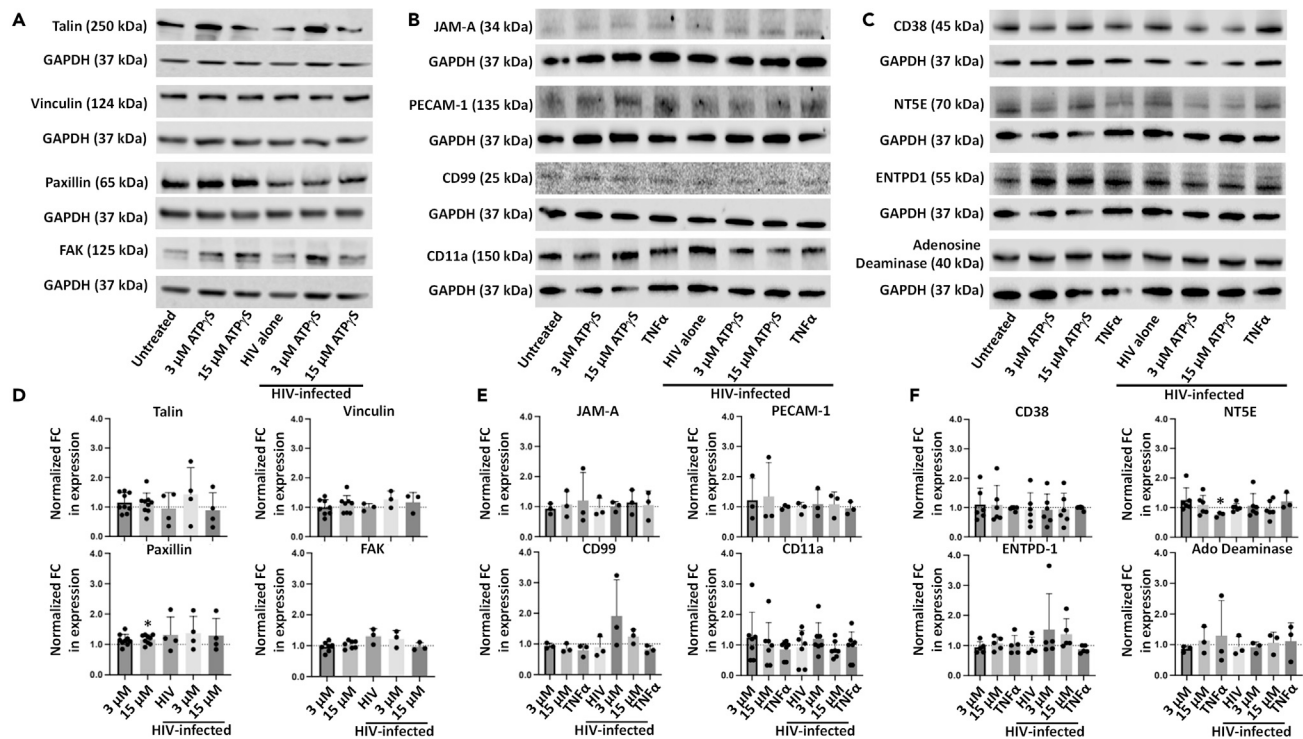


**Figure 4. Focal adhesion molecules, junctional proteins, and eATP metabolism enzyme expression are not significantly altered after acute ATPγS treatment of HIV-infected or uninfected PBMCs**

PBMCs were isolated from Leukopaks derived from healthy patients, then infected *in vitro* with HIV<sub>ADA</sub><sup>31–34</sup> or pNL(AD<sub>g</sub>) (10 ng/mL).<sup>35</sup> PBMCs (infected and uninfected) were either untreated or treated with 3 μM or 15 μM ATPγS (for four to five days), or TNFα (8–12 h) and used for Western blotting. TNFα was used as a positive control as it increases leukocyte attachment to endothelial cells.

(A) Representative Western blots for talin, vinculin, paxillin, and focal adhesion kinase (FAK); (B) JAM-A, PECAM-1, CD99, and CD11a; (C) CD38, NT5E/CD73, ENTPD1/CD39, and adenosine (ado) deaminase. GAPDH was used as a loading.

(D–F) correspond to the quantification of the Western blot data, target bands were normalized to GAPDH, then compared to corresponding untreated conditions, n = 3–9 independent experiments. Aside from the 1.15 ± 0.15-fold change in paxillin expression in the 15 μM ATPγS condition (n = 9, \*p < 0.05, compared to the untreated/uninfected condition). No significant differences were identified in uninfected/HIV-infected and 3 μM and 15 μM ATPγS-treated cells. As far as TNFα treatment, there was a significant decrease in NT5E expression, 0.76 ± 0.08 compared to untreated/uninfected (n = 3, \*p < 0.05). Experiments used at least three different donor Leukopaks. Data are represented as mean ± standard deviation. Significance was determined using Wilcoxon Signed Rank test. \*p < 0.05.

threshold at the EC-EC junction, hence the high discontinuity index. In contrast to this, JAM-A redistributed to the EC-EC junction for both 15 μM ATPγS (Figure 3W, n = 3, \*p < 0.0005, a discontinuity index of 0.20 ± 0.14 and 0.63 ± 0.19 for 15 μM ATPγS and untreated, respectively) and TNFα (Figure 3W, n = 3, \*p < 0.0005, a discontinuity index of 0.19 ± 0.12 and 0.63 ± 0.19 for TNFα and untreated, respectively). Figure 3X shows an example of the quantitation of JAM-A localization between two cells and Figures 3Y and 3Z demonstrate the JAM-A intensity along the EC-EC junction is above the cellular threshold for 15 μM, suggesting higher continuity due to protein redistribution. Overall, HAD-associated eATP treatment compromises JAM-A distribution, but similar to PECAM-1, the changes were mild.

### Adenosine triphosphate treatment does not alter the expression of critical adhesion, junctional, and adenosine triphosphate metabolism enzymes in uninfected and human immunodeficiency virus-infected peripheral blood mononuclear cells

A critical component of NeuroHIV, in addition to BBB integrity, is the transmigration of uninfected and HIV-infected leukocytes into the brain.<sup>30</sup> Peripheral blood mononuclear cells (PBMCs) were isolated from Leukopaks (healthy donors) and infected *in vitro* using the HIV<sub>ADA</sub> viral isolate<sup>31–34</sup> or molecular clone pNL(AD<sub>g</sub>) (an R5-pseudotyped NL4-3 clone).<sup>35</sup> After about one cycle of replication, 18–24 h after infection, treatment with ATPγS began (3 μM or 15 μM). After 5–6 days post-infection (4–5 days post-initiation of treatment), or 8–12 h post-TNFα treatment, cells were collected for subsequent experiments. We examined the total protein expression of focal adhesion proteins (talin, vinculin, paxillin, and focal adhesion kinase, FAK), molecules involved in attachment/adhesion (PECAM-1 and CD11a/LFA-1), junctional proteins (JAM-A and CD99), and eATP metabolism enzymes (CD38, NT5E/CD73, and ENTPD1/CD39) by Western blot (Figures 4A–4C) and flow cytometry (CD11a within Figures S3G and S3H). Focal adhesion molecules aid in facilitating integrin-cytoskeleton

interactions and modulate attachment to the extracellular matrix or other cells.<sup>36</sup> Western blots indicate that paxillin had a significant change in total expression in the 15  $\mu\text{M}$  ATP $\gamma\text{S}$ , a  $1.15 \pm 0.15$ -fold change compared to the untreated condition (Figures 4A and 4D,  $n = 9$ ,  $*p < 0.05$  compared to untreated). Aside from this result, we did not detect significant changes in FAK, vinculin, and talin in uninfected and HIV-infected cells in the presence of either 3  $\mu\text{M}$  or 15  $\mu\text{M}$  ATP $\gamma\text{S}$ . Analysis of critical adhesion and junctional molecules for leukocyte activation, adhesion, and transmigration indicated that none of the proteins analyzed had a significant change in total expression (Figures 4B and 4E). Among the eATP metabolism enzymes, only TNF $\alpha$  reduced NT5E/CD73 expression by  $0.76 \pm 0.08$ -fold change compared to untreated (Figure 4F,  $n = 3$ ,  $*p < 0.05$ ). Otherwise, there were no significant changes in total protein expression in response to 3  $\mu\text{M}$  or 15  $\mu\text{M}$  ATP $\gamma\text{S}$ . A reduction in CD73 expression was found upon the TNF $\alpha$  treatment of PBMCs.<sup>37</sup> FACS analyses confirmed our Western blot analysis for CD11a, indicating that HIV and ATP $\gamma\text{S}$  did not affect the surface expression of CD11a (Figures S3G and S3H). Overall, our data indicates that healthy and HAD-associated eATP concentrations (3  $\mu\text{M}$  and 15  $\mu\text{M}$  eATP, respectively) only result in minimal alterations in the expression and surface localization of molecules involved in leukocyte transmigration, cell adhesion, and eATP metabolism in the presence and absence of HIV infection.

### Extracellular adenosine triphosphate concentrations identified in people with human immunodeficiency virus and associated dementia trigger transcellular transmigration

A critical identifier of brain damage within PWH even in the current ART era is the localized CNS damage and leukocyte transmigration across the BBB.<sup>38,39</sup> Thus, we quantified leukocyte attachment and transmigration across BMVEC in the presence of chronic conditions observed within PWH, such as HIV infection and HAD-associated eATP. As described above, ATP $\gamma\text{S}$  treatment of BMVEC or PBMCs did not affect the expression of several key adhesion, junctional molecules, or MMP expression (see Figures 1, 2, 3, 4, S3, and S4). Our data indicated that the addition of 3  $\mu\text{M}$  or 15  $\mu\text{M}$  ATP $\gamma\text{S}$ -treated leukocytes to BMVEC exposed to the same treatment resulted in three different leukocyte phenotypes: attachment, paracellular, and transcellular transmigration (see Figures S3A–S3C for graphical representations of each morphology).

We determined that the time course of attachment, migration, and transmigration (paracellular or transcellular) reached a peak between 15 and 30 min depending on the donor (data not shown, analysis up to 2 h). The attachment was defined as a leukocyte-BMVEC interaction without significant changes in actin organization in BMVEC, a round leukocyte shape without cell polarization, a lack of localization to BMVEC cell-to-cell junctions, and a lack of VE-cadherin “cup” required for transcellular transmigration (Figure 5A, attachment, see red arrow). Paracellular transmigration was identified by the leukocyte localization at an endothelial/endothelial cell junction and leukocyte polarization (Figure 5B, paracellular, see yellow arrows). Transcellular transmigration was identified by the leukocyte localization at the same plane of the endothelial cell with changes in the actin fibers within the endothelial cell, polarization in leukocyte morphology, a VE-cadherin/caveolin-1 “cup” around the leukocyte, and part or the entire leukocyte within the endothelial cell (Figure 5C, transcellular, see white arrow and the XZ plane within the endothelial cell).

HIV infection of leukocytes in the presence of 3  $\mu\text{M}$  (healthy conditions) or 15  $\mu\text{M}$  (HAD-associated eATP) ATP $\gamma\text{S}$  increased leukocyte attachment to BMVEC (Figure 5D,  $n = 3$ ,  $*p < 0.0001$  compared to untreated/uninfected condition, the average leukocyte counts per field were: untreated -  $19 \pm 3$ , HIV -  $45 \pm 4$ , 3  $\mu\text{M}$  -  $33 \pm 6$ , 3  $\mu\text{M}$ +HIV -  $40 \pm 2$ , 15  $\mu\text{M}$ - $39 \pm 9$ , 15  $\mu\text{M}$ +HIV -  $33 \pm 3$ , TNF $\alpha$  -  $48 \pm 19$ , TNF $\alpha$ +HIV -  $41 \pm 3$ ). TNF $\alpha$  was used as a positive control, which resulted in enhanced attachment in uninfected and HIV-infected conditions (Figure 5D, TNF $\alpha$ ). HIV-infection increased attachment between the uninfected 3  $\mu\text{M}$  and the HIV-infected 3  $\mu\text{M}$  conditions (Figure 5D,  $n = 3$ ,  $\#p < 0.05$  uninfected and 3  $\mu\text{M}$  compared to HIV infected and 3  $\mu\text{M}$  condition, the average leukocyte counts per field were: 3  $\mu\text{M}$  -  $33 \pm 6$ , 3  $\mu\text{M}$ +HIV -  $40 \pm 2$ , respectively). Thus, ATP $\gamma\text{S}$  treatment in combination with HIV infection enhanced leukocyte attachment to BMVEC.

Quantification of paracellular transmigration phenotype indicates that the combination of HIV infection and 3  $\mu\text{M}$  ATP $\gamma\text{S}$  enhanced paracellular transmigration (Figure 5E,  $n = 3$ ,  $*p < 0.0001$ , with average an average number of leukocytes per field undergoing paracellular transmigration were  $9 \pm 3$  and  $23 \pm 4$  for untreated/uninfected and 3  $\mu\text{M}$  + HIV, respectively;  $n = 3$ ,  $\#p < 0.0001$ , 3  $\mu\text{M}$ , compared to 3  $\mu\text{M}$  + HIV, with average numbers of leukocytes are  $12 \pm 2$  and  $23 \pm 4$  for untreated 3  $\mu\text{M}$  and 3  $\mu\text{M}$  + HIV). TNF $\alpha$  was used as a positive control without HIV infection enhanced paracellular transmigration (Figure 5E,  $n = 3$ ,  $*p < 0.0001$ , with average an average number of leukocytes per field undergoing paracellular transmigration are  $9 \pm 3$  and  $25 \pm 5$  for untreated/uninfected and TNF $\alpha$ , respectively).

The quantification of transcellular leukocyte transmigration indicated that HIV-infected leukocytes and BMVEC exposed to HAD-associated eATP concentrations (15  $\mu\text{M}$ ) induced transcellular transmigration (Figure 5F,  $n = 3$ ,  $*p < 0.0001$ , the average count of  $0 \pm 0$  and  $23 \pm 3$  for untreated/uninfected and HIV-infected plus 15  $\mu\text{M}$  ATP $\gamma\text{S}$  conditions, respectively;  $\#p < 0.0001$  an average count of  $0 \pm 0$  and  $23 \pm 3$  for uninfected plus 15  $\mu\text{M}$  ATP $\gamma\text{S}$  and HIV-infected and 15  $\mu\text{M}$  ATP $\gamma\text{S}$  conditions, respectively). The combination of HIV infection and 15  $\mu\text{M}$  ATP $\gamma\text{S}$  was the only condition that triggered transcellular transmigration (Figure 5F). Overall, our data identified a unique mechanism of BBB transmigration associated with HIV infection and HAD-associated eATP, both essential components to detect the early onset of cognitive impairment within PWH.

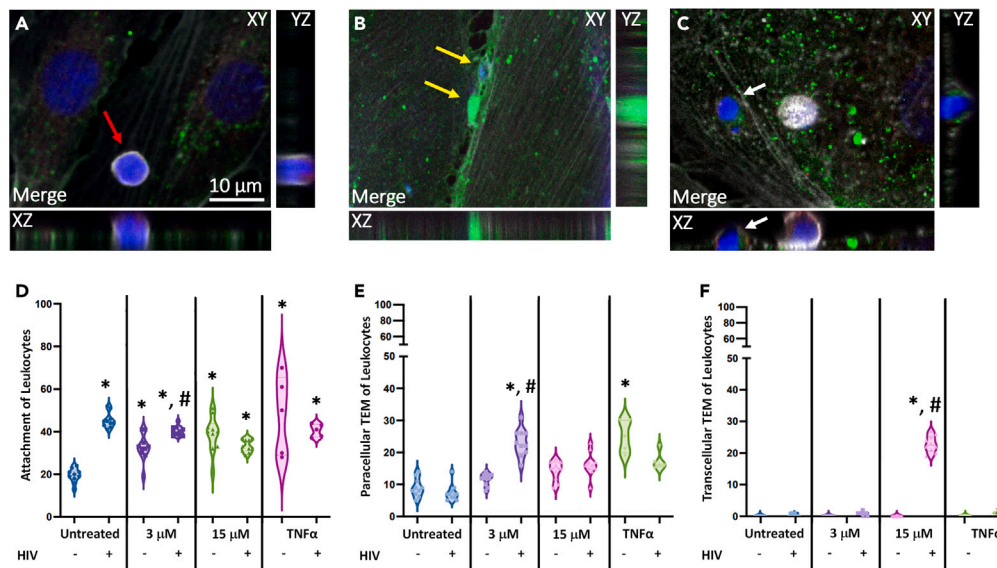


**Figure 5. Quantification of attachment and paracellular/transcellular transmigration upon HIV infection and treatment of 3  $\mu$ M and 15  $\mu$ M ATP $\gamma$ S, or TNF $\alpha$**

(A) representative 3D reconstruction of a leukocyte attached to an endothelial cell. YZ and XZ planes at the side of the image indicate that the attached leukocyte lacks polarization, see red arrow.

(B) representative 3D reconstruction of leukocytes in the process of paracellular transmigration (yellow arrows). YZ and XZ planes at the side of the image indicate leukocyte polarization and migration at the EC-EC junction.

(C) representative 3D reconstruction of a leukocyte in the process of transcellular transmigration. YZ and XZ planes at the side of the image indicate leukocyte polarization and endothelial cell cup formation, EC actin rearrangement, and migration through the endothelial cells, see white arrows.

(D) Quantification of attachment of leukocytes to BMVEC in untreated/treated and uninfected/HIV-infected conditions. ATP $\gamma$ S and/or HIV infection increase attachment ( $n = 3$ ,  $*p < 0.0001$  compared to untreated/uninfected condition, the average leukocyte counts per field were: untreated -  $19 \pm 3$ , HIV -  $45 \pm 4$ , 3  $\mu$ M -  $33 \pm 6$ , 3  $\mu$ M+HIV -  $40 \pm 2$ , 15  $\mu$ M -  $39 \pm 9$ , 15  $\mu$ M+HIV -  $33 \pm 3$ , TNF $\alpha$  -  $48 \pm 19$ , TNF $\alpha$ +HIV -  $41 \pm 3$ ). 3  $\mu$ M ATP $\gamma$ S further enhanced attachment in combination with HIV infection ( $n = 3$ ,  $\#p < 0.05$  compared to uninfected 3  $\mu$ M ATP $\gamma$ S, the average leukocyte counts per field were: 3  $\mu$ M -  $33 \pm 6$ , 3  $\mu$ M+HIV -  $40 \pm 2$ ). TNF $\alpha$  treatment was used as a positive control for endothelial activation and leukocyte attachment.

(E) Quantification of paracellular transmigration of uninfected/HIV-infected conditions in the presence and absence of 3  $\mu$ M or 15  $\mu$ M ATP $\gamma$ S. The combination of HIV and 3  $\mu$ M ATP $\gamma$ S enhanced paracellular transmigration ( $n = 3$ ,  $*p < 0.0001$ , with average an average number of leukocytes per field undergoing paracellular transmigration were  $9 \pm 3$  and  $23 \pm 4$  for untreated/uninfected and 3  $\mu$ M + HIV, respectively;  $\#p < 0.0001$ , 3  $\mu$ M, compared to 3  $\mu$ M + HIV, with average numbers of leukocytes are  $12 \pm 2$  and  $23 \pm 4$  for untreated 3  $\mu$ M and 3  $\mu$ M + HIV, respectively). TNF $\alpha$  was used as a positive control to induce paracellular transmigration without HIV infection enhanced paracellular transmigration (Figure 5E,  $n = 3$ ,  $*p < 0.0001$ , with average an average number of leukocytes per field undergoing paracellular transmigration are  $9 \pm 3$  and  $25 \pm 5$  for untreated/uninfected and TNF $\alpha$ , respectively).

(F) Quantification of transcellular transmigration. Only the combination of HIV-infected leukocytes and 15  $\mu$ M ATP $\gamma$ S (15  $\mu$ M corresponds to HAD-associated eATP) triggered transcellular transmigration ( $n = 3$ ,  $*p < 0.0001$ , the average count of  $0 \pm 0$  and  $23 \pm 3$  for untreated/uninfected and HIV-infected 15  $\mu$ M condition, respectively;  $\#p < 0.0001$  an average count of  $0 \pm 0$  and  $23 \pm 3$  for uninfected 15  $\mu$ M and HIV-infected 15  $\mu$ M conditions, respectively). TNF $\alpha$  treatment was unable to trigger transcellular transmigration. Data are represented as mean  $\pm$  standard deviation. Significance was determined using Wilcoxon Signed Rank test.  $*p < 0.0001$   $\#p \leq 0.05$ .

### Extracellular adenosine triphosphate concentrations identified in people with human immunodeficiency virus and associated dementia-mediated transcellular transmigration by a viral replication and chemokine (C-C motif) ligand-2 independent mechanism

Our published data demonstrated that HIV invasion into the brain involves the transmigration of HIV-infected leukocytes across the BBB by a CCL2-dependent mechanism during acute HIV infection.<sup>17</sup> In agreement with published data, CCL2 is elevated within the CSF of patients with HAD, which is the main chemoattractant for leukocyte recruitment into the brain.<sup>17,40</sup> However, in the current ART era, CCL2 concentrations are not elevated in aviremic patients, in contrast to viremic patients with a significantly higher concentration of CCL2 within serum.<sup>41</sup> This suggests that for PWH on ART that are diagnosed with HAND, there may be an alternative mechanism of leukocyte invasion into the brain that is CCL2 and HIV replication independent.

Quantification of HIV-p24 by enzyme-linked immunosorbent assay (ELISA) indicated that HIV infected the leukocytes in all the conditions, untreated, 3  $\mu$ M, and 15  $\mu$ M ATP $\gamma$ S had similar viral replication (data not shown,  $1.1 \pm 0.398$  for 3  $\mu$ M and  $1.19 \pm 0.305$  for 15  $\mu$ M ATP $\gamma$ S, fold change compared to infection alone,  $n = 3$ ). Prior to the coculture experiment, PBMCs were washed twice to remove any soluble HIV. Also, due to the short duration of the coculture experiments, no HIV-p24 was detected in the supernatant during the cocultures (data not shown). Quantification of CCL2 released by BMVEC did not show any changes in concentration, regardless of the number of passages cultured in the

presence of either concentration of ATP $\gamma$ S (Figure S4D,  $n = 3$ , 3  $\mu$ M and 15  $\mu$ M ATP $\gamma$ S conditions, compared to untreated). This finding is consistent with published results that show (24-h) 10  $\mu$ M ATP $\gamma$ S treatment of an endothelial cell line does not significantly increase the release of CCL2.<sup>42</sup> These data demonstrate that transcellular transmigration elicited by HIV and HAD-associated eATP (15  $\mu$ M) is not dependent on viral release and high CCL2, as we described in acute HIV conditions where transmigration was paracellular with significant changes in BBB permeability. Thus, the mechanism of transcellular transmigration elicited by HIV and HAD-associated eATP is different than acute infection.

### Extracellular adenosine triphosphate concentrations identified in people with human immunodeficiency virus and associated dementia-induced transcellular leukocyte transmigration by a junctional adhesion molecule-A and lymphocyte function-associated antigen 1-dependent mechanism

To determine the mechanisms of HIV and HAD-associated eATP-mediated transcellular transmigration, we examined the participation of key adhesion molecules involved in paracellular and transcellular transmigration such as JAM-A and CD99 using neutralizing antibodies or an LFA-1 mimetic peptide characterized to prevent leukocyte-associated LFA-1 binding to endothelial cells.<sup>43</sup> As controls, the same concentration of IgG isotype or a scrambled peptide was used. The neutralizing antibodies or mimetic peptides were added to the BMVECs 30 min before the addition of uninfected or HIV-infected leukocytes (in the presence of ATP $\gamma$ S treatment; Figure 6). For these experiments, leukocyte attachment (Figures 6A and 6D), paracellular (Figures 6B and 6D) and transcellular (Figures 6C and 6F) transmigration were quantified as presented in Figure 5. In uninfected conditions, JAM-A neutralizing antibodies promoted the attachment of uninfected leukocytes, in combination with 3  $\mu$ M or 15  $\mu$ M ATP $\gamma$ S treatment (Figure 6A,  $*p < 0.0001$ , the average number of attached leukocytes within the uninfected 3  $\mu$ M ATP $\gamma$ S conditions were  $32 \pm 6$  and  $51 \pm 7$  for the IgG treatment and  $\alpha$ JAM-A condition, respectively; for the 15  $\mu$ M ATP $\gamma$ S condition, the average number of leukocytes attached were  $38 \pm 9$  and  $58 \pm 7$  for the IgG treatment and  $\alpha$ JAM-A condition, respectively). JAM-A neutralizing antibodies prevented paracellular transmigration of uninfected leukocytes elicited by TNF $\alpha$  treatment (Figure 6B,  $*p < 0.0001$ , the average number of leukocytes was  $25 \pm 5$  and  $4 \pm 2$  for IgG and  $\alpha$ JAM-A conditions, respectively). Thus, the differences were not due to overall changes in attachment. Neutralizing antibodies to JAM-A or CD99 did not enhance transcellular transmigration in uninfected conditions. This supports the data in Figure 5 that enhanced transcellular transmigration requires HIV infection and HAD-associated eATP to occur (Figure 6C, no transcellular transmigration detected).

In contrast, in the HIV-infected and 3  $\mu$ M ATP $\gamma$ S condition, neutralizing antibodies to JAM-A prevented attachment (Figure 6D Representative experiment,  $*p < 0.0001$ , the average numbers of attached leukocytes were  $51 \pm 6$  and  $31 \pm 4$  for IgG and  $\alpha$ JAM-A conditions, respectively). Neutralizing antibodies to JAM-A also enhanced paracellular transmigration within the 3  $\mu$ M ATP $\gamma$ S condition (Figure 6E,  $*p < 0.0001$ , the average number of leukocytes are  $22 \pm 2$  and  $35 \pm 2$  for IgG and  $\alpha$ JAM-A, respectively) suggesting the unique participation of JAM-A during brain invasion elicited by HIV infection and the physiological concentration of eATP. Most importantly, blocking JAM-A prevented transcellular transmigration induced by HIV infection and HAD-associated eATP (Figure 6F representative experiment,  $n = 4$ ,  $*p < 0.0001$ , the average numbers of leukocytes were  $21 \pm 6$  and  $6 \pm 2$  for IgG and  $\alpha$ JAM-A, respectively). CD99-neutralizing antibodies increased transcellular transmigration within the HIV-infected 15  $\mu$ M ATP $\gamma$ S condition (Figure 6F representative experiment,  $n = 3$ ,  $*p < 0.0001$ , the average numbers of leukocytes were  $22 \pm 2$  and  $31 \pm 4$  for IgG and  $\alpha$ CD99, respectively). Due to CD99 being one of the last adhesion molecules involved in leukocyte transmigration it is likely not involved in attachment and paracellular transmigration at our observed time frame.<sup>44</sup>

To elucidate the role of LFA-1 within transcellular migration, we utilized a mimetic peptide to compete for the LFA-1 interaction between leukocytes and BMVEC.<sup>43</sup> When the LFA-1 mimetic peptide (LFA-pep) was present, there was a reduction in leukocyte attachment (Figure 7A representative experiment,  $n = 3$ ,  $*p < 0.0004$ , the average number of attached leukocytes were  $35 \pm 4$  and  $28 \pm 5$  for scrambled and LFA-1-peptide, respectively), as well as a complete abolishing of transcellular transmigration in HIV and HAD-associated eATP condition (Figure 7A representative experiment,  $n = 3$ ,  $*p < 0.0001$ , the average number of leukocytes were  $21 \pm 6$  and  $1 \pm 0.5$  per field for the scrambled and LFA-1 peptide, respectively). Overall, HIV-mediated transmigration in response to HAD-associated eATP was JAM-A and LFA-1 dependent.

### Extracellular adenosine triphosphate identified in human immunodeficiency virus infection and associated dementia selectively promotes the transmigration of human immunodeficiency virus-infected leukocytes

To determine whether the transmigrating leukocytes were HIV-infected, we stained for HIV-p24. Quantification of attachment and paracellular transmigration in HIV-infected conditions indicated that most leukocytes attached or in the process of paracellular transmigration were uninfected (Figure 7B, representative donor,  $n = 3$ , white bars). However, most leukocytes undergoing transcellular transmigration were HIV-infected (HIV-p24 positive, Figure 7B, black bar). This data indicated that HIV-infected cells treated with HAD-associated eATP selectively undergo transcellular transmigration to cross the BBB. The transcellular leukocyte transmigration triggered by HIV and HAD-associated eATP was sensitive to neutralizing antibodies to JAM-A reducing the total leukocyte number of HIV-infected cells undergoing transcellular transmigration (Figure 7B,  $\alpha$ JAM-A/Trans,  $n = 3$ , representative donor). The JAM-A neutralizing antibodies also prevented the proportion of HIV-infected leukocytes undergoing transcellular transmigration from  $80 \pm 14\%$  to  $43 \pm 7.8\%$  (Figure 7C,  $n = 3$ ,  $*p < 0.0015$ ). Non-immune IgG did not affect the transmigration or selection compared to untreated co-cultures. Overall, our data demonstrated that most HIV-infected leukocytes underwent transcellular transmigration elicited by HAD-associated eATP and HIV infection, dependent on JAM-A and LFA-1.

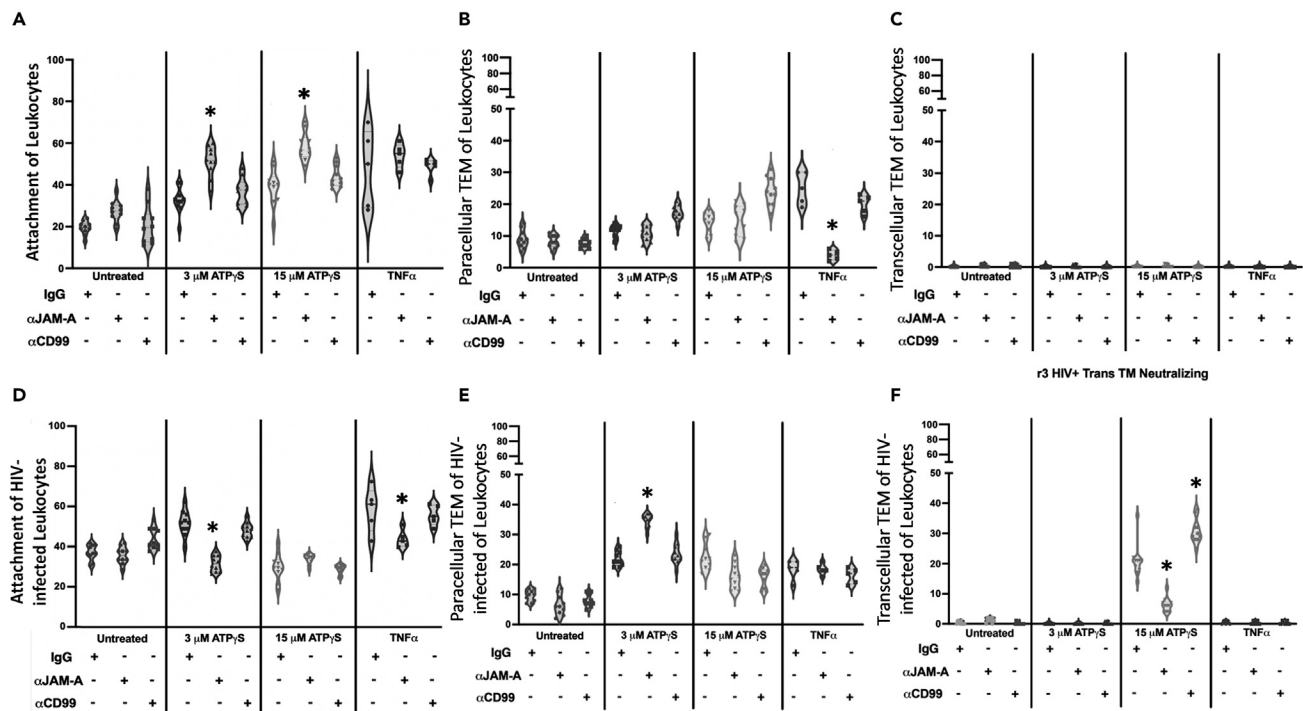


**Figure 6. JAM-A, but not CD99, is a critical adhesion molecule for attachment, and transcellular leukocyte transmigration**

BMVEC were pre-treated with neutralizing JAM-A or CD99 antibodies or the corresponding isotype control (IgG) for 30 min and then identical numbers of leukocytes were added and allowed to attach and undergo transmigration for 30 min. Leukocytes were stained for CD4, and endothelial cells were stained for VE-cadherin described in Figure 5, to quantify attachment, and either paracellular or transcellular transmigration.

(A–C) correspond to attachment, paracellular, and transcellular transmigration, respectively, in uninfected conditions. JAM-A neutralizing antibodies enhanced the attachment of 3 μM and 15 μM ATPγS treated leukocytes ( $n = 3$ ,  $*p < 0.0001$ , the average number of attached leukocytes within the uninfected, 3 μM ATPγS conditions were  $32 \pm 6$  and  $51 \pm 7$  for the IgG treatment and αJAM-A condition, respectively; for the 15 μM ATPγS condition, the average number of leukocytes attached within the IgG condition were  $38 \pm 9$  and within the αJAM-A condition,  $58 \pm 7$  leukocytes were attached). Blocking JAM-A also reduced paracellular transmigration within the TNFα condition ( $n = 3$ ,  $*p < 0.0001$ , the average number of leukocytes was  $25 \pm 5$  and  $4 \pm 2$  for IgG and αJAM-A conditions, respectively, the differences observed were not due to changes in attachment). No transcellular transmigration was observed within any of the uninfected conditions.

(D–F) correspond to attachment, paracellular, and transcellular transmigration, respectively, in HIV-infected conditions. In contrast to uninfected conditions, JAM-A neutralizing antibodies prevented attachment induced by 3 μM ATPγS ( $n = 3$ ,  $*p < 0.0001$ , the average number of attached leukocytes was  $51 \pm 6$  and  $31 \pm 4$  for IgG and αJAM-A conditions, respectively) and TNFα treatment ( $n = 3$ ,  $*p < 0.0001$  with average number of attached leukocytes were  $22 \pm 2$  and  $35 \pm 2$  for IgG and αJAM-A conditions, respectively). JAM-A neutralizing antibodies exacerbated the number of leukocytes undergoing paracellular transmigration within the 3 μM ATPγS condition ( $n = 3$ ,  $*p < 0.0001$ , the average number of leukocytes are  $21 \pm 6$  and  $6 \pm 2$  for IgG and αJAM-A, respectively). More importantly, JAM-A neutralizing antibodies, but not CD99 antibodies (blocking CD99 increased transcellular transmigration;  $n = 3$ ,  $*p < 0.0001$ , the average number of leukocytes was  $22 \pm 2$  and  $31 \pm 4$  leukocytes per field for IgG and αCD99, respectively), prevented transcellular transmigration induced by 15 μM ATPγS and HIV infection ( $n = 4$ ,  $*p < 0.0001$ , the average number of leukocytes was  $22 \pm 6$  and  $7 \pm 2$  leukocytes per field for IgG and αJAM-A, respectively). An isotype-matched control antibody (IgG) did not affect attachment or transmigration. Data are represented as mean  $\pm$  standard deviation. Significance was determined using the Wilcoxon Signed Rank test.  $*p < 0.0001$ .

## DISCUSSION

Our data identified that PWH under ART with the onset of cognitive impairment had increased ATP levels in the circulation.<sup>7</sup> We propose that ATP within serum could be a biomarker of cognitive impairment in PWH and also a contributor to the brain pathogenesis observed in PWH despite the lack of systemic replication.<sup>7</sup> Normally, eATP is degraded by a series of redundant enzymes to keep its concentration within the sub-micromolar range, but within PWH, these mechanisms are poorly regulated. Only recently, the laboratory of Dr. Pillai demonstrated that viral reservoirs have a unique expression signature of CD73, IL-8, and CD39<sup>45</sup>. Blocking CD73 or adenosine receptors facilitates latent HIV reactivation linking purinergic signaling with viral quiescence.<sup>45</sup> eATP is considered a key component of the “find me” signal for clear dying cells under homeostatic conditions.<sup>46</sup> ATP, as well as UTP, and fractalkine, are the main chemoattractants for monocytes.<sup>46,47</sup> ATP concentrations ( $\sim 100$  nM or higher) are released by apoptotic lymphocytes<sup>47</sup> and necrotic cells; under physiological conditions, eATP is rapidly degraded (in minutes) to avoid overactivation of purinergic receptors and serves as a chemotactic signal for phagocyte-mediated cell clearance.<sup>46</sup> In contrast, high eATP concentrations (0.5–1 mM) can trigger apoptosis by a P2X<sub>7</sub>-mediated mechanism.<sup>48</sup> eATP is a potent inflammatory molecule or damage-associated molecular pattern (DAMP), ATP is elevated within the serum of multiple inflammatory conditions such

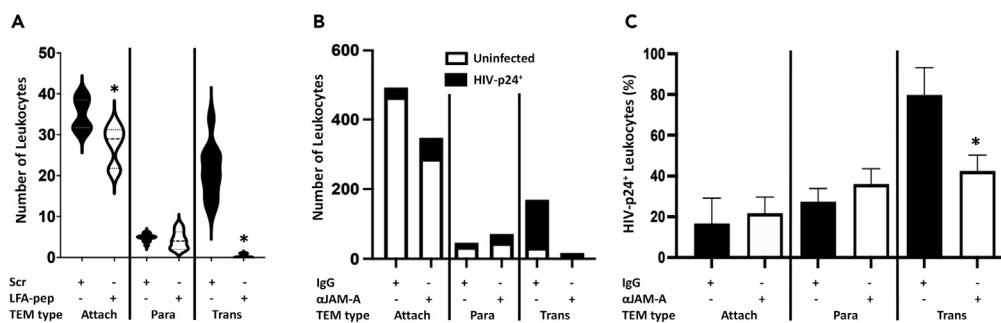


### Figure 7. 15 $\mu\text{M}$ ATP $\gamma\text{S}$ -treated HIV-infected leukocytes undergo transcellular transmigration dependent on a JAM-A and LFA-1-based mechanism

To quantify the ratios of uninfected and HIV-infected cells during transcellular transmigration, we stained for HIV-p24 in addition to the markers described in Figures 5 and 6 while blocking JAM-A or blocking endothelial cell JAM-A/LFA-1 binding with leukocyte LFA-1 with an LFA-1 mimetic peptide.

(A) Leukocyte attachment ( $n = 3$ , representative experiment shown,  $*p < 0.0004$ , average number of attached leukocytes was  $35 \pm 4$  and  $28 \pm 5$  for scrambled and LFA-1-peptide, respectively) and transcellular transmigration induced by HIV and 15  $\mu\text{M}$  ATP $\gamma\text{S}$  are highly dependent on an LFA-1-dependent interaction ( $n = 3$ ,  $*p < 0.0001$  LFA-1-peptide compared to scrambled, an average of  $21 \pm 6$  and  $1 \pm 0.5$  for scramble and LFA-1-peptide, respectively).

(B) Total numbers of uninfected and HIV-infected leukocytes attached or undergoing paracellular/transcellular transmigration induced by HIV and 15  $\mu\text{M}$  ATP $\gamma\text{S}$ . The attached leukocytes were mostly uninfected cells (white bars) with a small contribution of HIV-infected cells (black bars); JAM-A reduced the total number of attached cells (representative donor, 491 and 347 attached leukocytes for IgG and  $\alpha\text{JAM-A}$ , respectively). Leukocytes undergoing paracellular transmigration were also mostly uninfected. HIV-infected cells selectively underwent transcellular transmigration. JAM-A neutralizing antibodies reduced the total number of leukocytes undergoing transcellular transmigration ( $n = 3$ , IgG compared to  $\alpha\text{JAM-A}$ , 136 HIV-infected of a total of 169 leukocytes for IgG, compared to 6 HIV-infected of a total of 15 leukocytes for  $\alpha\text{JAM-A}$ ).

(C) Blocking JAM-A reduces the proportion of HIV-infected cells undergoing transcellular transmigration ( $n = 3$ ,  $*p < 0.0015$ ,  $80 \pm 14\%$  to  $43 \pm 8\%$  HIV-infected cells undergoing transcellular transmigration for IgG and JAM-A, respectively). Data are represented as mean  $\pm$  standard deviation. Significance was determined using the Wilcoxon Signed Rank test.  $*p \leq 0.006$ .

as rheumatoid arthritis and atherosclerosis resulting in leukocyte and endothelial activation.<sup>49–51</sup> However, most of these inflammatory mechanisms are associated with cell turnover and acute inflammation.

Our data indicated that all PWH have high levels of ATP in the circulation, suggesting a chronic inflammatory state, independent of systemic viral replication or associated comorbidities that can support vascular disease in PWH as described above.<sup>7</sup> Additionally, serum concentration of ATP over 15  $\mu\text{M}$  is associated with severe cognitive impairment suggesting that ATP is not only a potential biomarker of cognitive impairment but also a likely contributor to HAND progression.<sup>7</sup> Within acute HIV conditions, HIV binding to CD4/CCR5/CXCR4 resulted in Panx-1 channel opening and ATP release into the extracellular space to activate purinergic receptors to accelerate HIV entry and other steps for replication.<sup>8,9</sup> However, in acute HIV and SARS-CoV-2 conditions, eATP stability was short and eATP lasted only a few minutes as determined by chemiluminescence.<sup>9,52</sup> A critical question is: why eATP is elevated and stable within the serum of PWH? Our data using PBMCs from aviremic PWH indicated that Panx-1 channels spontaneously release ATP, contributing to serum ATP, but it is likely other cell types are involved.<sup>7</sup> Our analysis of eATP degrading enzymes did not show large differences in NT5E (CD73), ENTPD1 (CD39), adenosine deaminase, and CD38 upon HAD-associated eATP treatment in PBMCs and endothelial cells. The exception was the significant increase in adenosine deaminase expression in the HAD-associated eATP treatment of BMVEC. Thus, we propose those cells become adapted to chronic eATP.

The endothelium, leukocytes, and soluble ATPases including those within both the CD39 and CD73 families are key participants in the maintenance of anti-inflammatory and anti-thrombotic state in the vasculature by the fast nucleotide inactivation via stepwise reaction: ATP/ADP/AMP/adenosine (ADP, adenosine diphosphate and AMP, adenosine monophosphate).<sup>53</sup> Adenosine is anti-inflammatory and prevents excessive tissue damage mediated by the overactivation of purinergic receptors<sup>54</sup> by inhibiting cytokine release and expression of E-selectin and other adhesion molecules that promote transmigration.<sup>55</sup> Our mass spectrometry data suggests that the concentrations of ATP (five to 10-fold higher, relative to uninfected), ADP (10-fold higher, relative to uninfected), and AMP (5-fold higher, relative to uninfected) are elevated in the serum of PWH; however, adenosine within the serum is not significantly different within PWH, compared to uninfected (unpublished data). This would suggest that in addition to the persistent ATP release by cells, there is dysfunction of CD39 and CD73 due to their roles in catabolizing ATP/ADP into AMP, and AMP into adenosine, respectively. Similarly, cells chronically infected with HIV accumulate intracellular inositol triphosphate species.<sup>56</sup> Both inositol triphosphate and ATP contain high energy phosphate groups and during chronic HIV infection both accumulate to high concentrations and cells are seemingly unable to catabolize these molecules.<sup>56</sup>

The main consequences of high eATP are likely either constant activation or desensitization of the purinergic system to their ligands. Desensitization of purinergic receptors through repeated or sustained activation has been documented by several groups.<sup>57,58</sup> The consequences of aberrant purinergic signaling in PWH can be significant for several comorbidities including Alzheimer's disease, immune activation, and vascular disease.<sup>59–61</sup> Data from atherosclerosis studies indicates that P2Y and P2X receptor activation triggers the attachment of leukocytes and platelets to the vessel wall.<sup>62–64</sup> Drugs such as Prasugrel (anticoagulant) or Clopidogrel (a P2Y<sub>12</sub> inhibitor) decrease platelet attachment and atheroma formation.<sup>65</sup> CD8<sup>+</sup> T lymphocytes are implicated in protecting from atherosclerosis pathogenesis in MHC class

I-restricted activity.<sup>63</sup> The role of these cells is attributed to CD39 expression in reducing interferon gamma and TNF $\alpha$  secretion in atherosclerosis lesions.<sup>66</sup> This is an example of the involvement of the purinergic system in immune activation and endothelial compromise.

In HIV infection, it has been described that activated platelets binding to CD8<sup>+</sup> and CD4<sup>+</sup> T cells prevent proper activation and control long-term immune dysfunction.<sup>67</sup> However, whether these mechanisms are mediated by eATP or chronic purinergic receptor activation is not well described. Our data indicate that healthy eATP and HAD-associated eATP levels did not change the expression and distribution of key adhesion and junctional molecules, suggesting an adaptation. Normally, endothelial or leukocyte exposure to eATP or other inflammatory activators results in the abnormal expression and distribution of VCAM-1 resulting in leukocyte adhesion to the endothelium,<sup>68</sup> release of nitric oxide, prostaglandin I<sub>2</sub>, and endothelium-derived hyperpolarizing factor, as well as altered vasodilation.<sup>69,70</sup> Overall, we did not observe changes in key adhesion and junctional proteins in BMVEC or uninfected and HIV-infected leukocytes treated with eATP examined separately, suggesting a mild effect of eATP and HIV infection in each cell type.

However, the main finding of our article corresponds to the mechanism triggered by eATP concentrations identified in PWH with the cognitive impairment-triggered transcellular transmigration of mainly HIV-infected leukocytes across the BBB. In the current ART era, brain damage has been associated with cognitive impairment and depression-like behaviors by a mechanism of chronic neuroinflammation that is not associated with systemic viral replication but rather with the presence of viral reservoirs and bystander cell activation.<sup>56,71</sup> Neurofilament light chain (NFL),  $\beta$ -amyloid<sub>1-42</sub>, neopterin, CCL2, and sCD14 within either serum or CSF have been proposed, however, they are robust indicators of only the most severe neurocognitive impairment.<sup>17,72,73</sup> Our data indicated that serum ATP could be an early predictor for screening PWH for cognitive impairment.<sup>7</sup> Currently, brain damage in the current ART era is subtle, and brain imaging studies show white and gray matter lesions are highly localized, as suggested by several groups.<sup>38,39</sup> These subtle lesions have been associated with the presence of viral reservoirs and inflammation, synapto-dendritic injury, vascular compromise, demyelination, and localized leukocyte transmigration.<sup>38,39</sup> Overall, these structural and functional changes cannot be linked to current biomarkers within CSF or serum. Thus, the mechanisms of spatial and localized damage are unknown.

The process of transendothelial migration through blood vessels relies on several interactions between integrins, selectins, and cell adhesion molecules.<sup>14</sup> Although our treatment of 15  $\mu$ M ATP $\gamma$ S did not alter the total expression or surface expression of cell adhesion molecules, HAD-associated eATP affected the localization of PECAM-1 and JAM-A at the EC-EC junctions. The deletion of PECAM-1 within the context of transendothelial migration leads to an increase in the transcellular migration of CD4<sup>+</sup> T cells through an endothelial cell monolayer; the decrease in the localization of PECAM-1 to the EC-EC junction within the 15  $\mu$ M ATP $\gamma$ S condition could promote transcellular transmigration over paracellular as previously described.<sup>74</sup> During HIV infection, however, PECAM-1 is actively shed by PBMCs when treated with CCL2, and due to PECAM-1 shedding, homophilic interactions between BMVECs are likely disrupted, potentially promoting paracellular transmigration over transcellular transmigration.<sup>28</sup> Within our study, there is a lack of soluble PECAM-1 released from PBMCs, as they are washed out before addition to BMVECs, and CCL2 release is not increased upon the ATP $\gamma$ S treatment of BMVEC, a distinct difference from the study referenced.<sup>28</sup>

In contrast to PECAM-1, JAM-A was redistributed to cellular junctions within the 15  $\mu$ M ATP $\gamma$ S condition, similar to previous literature using human umbilical cord endothelial cells treated with TNF $\alpha$  and interferon-gamma.<sup>75</sup> This contrasts with other publications that see JAM-A at the cellular junctions in resting conditions but see redistribution from these junctions when endothelial cells are treated with CCL2.<sup>76</sup> Within our results, we do not supplement CCL2 for either the transmigration assay nor the ATP $\gamma$ S treatments of BMVEC/PBMCs, making our results distinct from the referenced study, as well as the BBB leukocyte transmigration during acute infection.<sup>17,28,76</sup> Regarding the role of JAM-A in the transcellular transmigration of leukocytes within the 15  $\mu$ M ATP $\gamma$ S condition using HIV-infected PBMCs, it is apparent that it plays a role in transcellular transmigration but not attachment. The exception is that within both the 3  $\mu$ M ATP $\gamma$ S and TNF $\alpha$  conditions with HIV-infected leukocytes, there was a significant reduction in the attachment of leukocytes when JAM-A was blocked. This could suggest that within the 15  $\mu$ M ATP $\gamma$ S condition, either the cell adhesion molecules or integrins involved in initial attachment may not be the same in this condition, compared to the 3  $\mu$ M ATP $\gamma$ S and TNF $\alpha$  conditions. The phenomena of the blocking of JAM-A with differing results across treatments are not exclusive to the results using HIV-infected leukocytes as there is an increase in attachment among both 3  $\mu$ M ATP $\gamma$ S and 15  $\mu$ M ATP $\gamma$ S conditions, relative to the untreated condition. The increase in attachment with HIV-infected leukocytes is not present within the TNF $\alpha$  treatment. It is perhaps the engagement of the anti-JAM-A antibody to the endothelial cell JAM-A at adherens junctions that disrupts homophilic interactions and subsequently allows for an increase in surface area, which allows for an increase in attachment. When human umbilical vein endothelial cells (HUVECs) are treated with TNF $\alpha$ , adherens junctions undergo remodeling and become more discontinuous as the surface area of HUVECs increases.<sup>77,78</sup> The decrease in adherens junction association and increase in surface area would be conducive for non-JAM-A mediated interactions with uninfected leukocytes.

Despite a lack of a change in CD99, JAM-A, and LFA-1 expression within leukocytes during HIV infection, we characterized their contribution to attachment, and paracellular and transcellular transmigration triggered by HIV and HAD-associated eATP. Blocking antibodies for JAM-A and an LFA-1-mimetic peptide prevented the transcellular transmigration of HIV-infected leukocytes. This mechanism is different than other diseases such as hypertension and atherosclerosis where JAM-A is implicated in paracellular TEM.<sup>79,80</sup> Similarly, there is a divergence from how ALCAM functions within leukocyte transmigration within allograft rejection, as well as encephalitic conditions, compared to our reported results due to its primarily playing a role in leukocyte retention in tissue.<sup>81</sup> JAM-A is a critical component of HIV entry into the brain during acute infection,<sup>19</sup> but also during chronic conditions, thus, we propose that a JAM-A/LFA-1 blockage strategy could limit the devastating effects of HIV and leukocyte invasion into the brain. Serum ATP as a biomarker of cognitive decline and contributor to leukocyte brain transmigration provides a unique opportunity to target JAM-A/LFA-1, as well as the release of ATP, and downstream signaling through

purinergic receptors to treat HAND. The potential of targeting purinergic signaling to reduce leukocyte invasion into the brain has been shown by several animal models, including intracerebral hemorrhage and ischemic stroke.<sup>82,83</sup> Our data has also shown promise to reduce leukocyte transmigration through an *in vitro* BBB cell culture model by the inhibition of Panx-1.<sup>7</sup> Lastly, our data also show that HIV-induced synaptic-dendritic pruning is reduced when Panx-1 is inhibited, preserving complex dendritic spines within an acute SIV infection model.<sup>11</sup> Thus, targeting either the release of ATP through Panx-1 or the downstream effects of purinergic signaling within circulation are both viable strategies for treating HAND.

Our data demonstrate a shift from paracellular transmigration in acute HIV conditions<sup>17</sup> into transcellular transmigration dependent on HIV infection and eATP. In several neuroinflammatory diseases, BBB permeability is increased and promotes the infiltration of leukocytes into the brain through paracellular or transcellular mechanisms.<sup>74,84,85</sup> Transcellular migration increases neuroinflammation and has been described in multiple sclerosis,<sup>85</sup> however, the molecular mechanisms are not fully identified. However, studies with neutrophils and transcellular migration suggest that diapedesis begins ICAM-1, VCAM-1, and actin becomes concentrated along the endothelial membrane surrounding the leukocyte forming a “cup” around them.<sup>15,20</sup> As denoted in our confocal images, endothelial processes form around the leukocyte and leukocytes extend filopodia-like projections into the endothelial cells, as others have published.<sup>20</sup>

However, how the endothelial cells select mostly HIV-infected cells is unknown and likely is related to a particular leukocyte population or residual viral replication resulting in the enhanced expression of specific adhesion molecules to support transcellular transmigration. We believe that HIV and eATP triggering the transcellular transmigration of HIV-infected leukocytes into the brain correspond to a selective method of chronic neuroinflammation. Several groups indicate that transcellular migration could be dependent on PECAM-1 and CD99<sup>44</sup>, however, our data indicates that PECAM-1 is not upregulated or cleaved, and neutralizing antibodies to CD99 did not affect transcellular leukocyte migration triggered by HIV and eATP. It has been proposed that transcellular migration may occur or is promoted if leukocytes have difficulty reaching the cell-to-cell junctions.<sup>44</sup> However, our data demonstrates that HIV-infected cells selectively undergo transcellular transmigration even in the presence of comparable attachment and paracellular transmigration. In neutrophils deficient in CD11b/CD18, paracellular migration was compromised due to the inability to locomote along the endothelial surface.<sup>86</sup> In our data, JAM-A and LFA-1 were essential to promote transcellular transmigration and the selectivity of HIV-infected cells.

Our results are the first to provide data for the concentration of ATP within serum to be a biomarker and contributor of HAND within PWH. This is indicated by the increase in the transendothelial migration of leukocytes through BMVECs after exposure to HAD-associated eATP. Further studies are warranted to understand the dysregulation of ATP within the serum of PWH and identify the purinergic receptors involved in the dysregulation of the BBB and leukocytes that could be a target for therapeutic intervention for HAND.

### Limitations of the study

Several questions remain for future studies including the role of different ART types, comorbidities, the leukocyte selection mechanisms for transcellular migration, and whether viral reservoirs exploit similar mechanisms for self renewal. As indicated in the [introduction](#), HIV damage in the PWH under ART is highly localized, thus, how an specific area become susceptible to invasion? is unknown. Future experiments in human tissues, non-human primates, or humanized mice tissues could provide answers to these questions. The identification of the purinergic receptors involved in transcellular leukocyte migration is essential for future pre- and clinical studies. ATP as a biomarker and contributor to CNS damage could provide exciting avenues to prevent the devastating consequences of cognitive decline in at least half of the HIV-infected population.

### STAR★METHODS

Detailed methods are provided in the online version of this paper and include the following:

- [KEY RESOURCES TABLE](#)
- [RESOURCE AVAILABILITY](#)
  - Lead contact
  - Materials availability
  - Data and code availability
- [EXPERIMENTAL MODEL AND STUDY PARTICIPANT DETAILS](#)
  - Cell culture
- [METHOD DETAILS](#)
  - BMVEC cell culture
  - PBMC culture
  - Establishment of acute ATP-treated cultures
  - HIV-p24 and CCL2 ELISA
  - BMVEC and PBMC coculture
  - Criteria and quantification of adhesion and trans migratory phenotypes
  - Co-culture blocking assay
  - Western blotting
  - Immunofluorescence
  - Immunofluorescence quantitation and analysis

- Flow cytometry
- **QUANTIFICATION AND STATISTICAL ANALYSIS**

## SUPPLEMENTAL INFORMATION

Supplemental information can be found online at <https://doi.org/10.1016/j.isci.2024.109236>.

## ACKNOWLEDGMENTS

This work was funded by the National Institute of Mental Health grant, MH128082, the National Institute of Neurological Disorders and Stroke, NS105584, and UTMB internal funding (to E. A. E.). The following reagents were obtained through the NIH AIDS Reagent Program, Division of AIDS, NIAID, NIH: HIV-1 NL4-3 AD8 Infectious Molecular Clone, pNL(AD8), from Dr. Eric O. Freed and HIV-1 ADA Virus from Dr. Howard Gendelman.

## AUTHOR CONTRIBUTIONS

Conceptualization: C.H., A.M.G., and E.A. E.  
 Investigation: C.H., A.M.G., and E.A.E.  
 Funding acquisition: E.A.E.  
 Project administration: E.A.E.  
 Supervision: E.A.E.  
 Writing – original draft: C.H., A.M.G., and E.A.E.  
 Writing, review, and editing: C.H., A.M.G., and E.A.E.  
 All authors discussed the results and commented on them.

## DECLARATION OF INTERESTS

The authors do not have any conflicts of interest.

Received: November 6, 2023

Revised: December 18, 2023

Accepted: February 9, 2024

Published: February 15, 2024

## REFERENCES

- Saylor, D., Dickens, A.M., Sacktor, N., Haughey, N., Slusher, B., Pletnikov, M., Mankowski, J.L., Brown, A., Volsky, D.J., and McArthur, J.C. (2016). HIV-associated neurocognitive disorder—pathogenesis and prospects for treatment. *Nat. Rev. Neurol.* *12*, 234–248. <https://doi.org/10.1038/nrneurol.2016.27>.
- Wei, J., Hou, J., Su, B., Jiang, T., Guo, C., Wang, W., Zhang, Y., Chang, B., Wu, H., and Zhang, T. (2020). The Prevalence of Frascati-Criteria-Based HIV-Associated Neurocognitive Disorder (HAND) in HIV-Infected Adults: A Systematic Review and Meta-Analysis. *Front. Neurol.* *11*, 581346. <https://doi.org/10.3389/fneur.2020.581346>.
- Simioni, S., Cavassini, M., Annoni, J.M., Rimbault Abraham, A., Bourquin, I., Schiffer, V., Calmy, A., Chave, J.P., Giacobini, E., Hirschel, B., and Du Pasquier, R.A. (2010). Cognitive dysfunction in HIV patients despite long-standing suppression of viremia. *AIDS* *24*, 1243–1250. <https://doi.org/10.1097/QAD.0b013e3283354a7b>.
- Ellis, R.J., Chenna, A., Petropoulos, C.J., Lie, Y., Curanovic, D., Crescini, M., Winslow, J., Sundermann, E., Tang, B., and Letendre, S.L. (2022). Higher cerebrospinal fluid biomarkers of neuronal injury in HIV-associated neurocognitive impairment. *J. Neurovirol.* *28*, 438–445. <https://doi.org/10.1007/s13365-022-01081-4>.
- Lyons, J.L., Uno, H., Ancuta, P., Kamat, A., Moore, D.J., Singer, E.J., Morgello, S., and Gabuzda, D. (2011). Plasma sCD14 is a biomarker associated with impaired neurocognitive test performance in attention and learning domains in HIV infection. *J. Acquir. Immune Defic. Syndr.* *57*, 371–379. <https://doi.org/10.1097/QAI.0b013e3282237e54>.
- Burdo, T.H., Weiffenbach, A., Woods, S.P., Letendre, S., Ellis, R.J., and Williams, K.C. (2013). Elevated sCD163 in plasma but not cerebrospinal fluid is a marker of neurocognitive impairment in HIV infection. *AIDS* *27*, 1387–1395. <https://doi.org/10.1097/QAD.0b013e32836010bd>.
- Velasquez, S., Prevedel, L., Valdebenito, S., Gorska, A.M., Golovko, M., Khan, N., Geiger, J., and Eugenin, E.A. (2020). Circulating levels of ATP is a biomarker of HIV cognitive impairment. *EBioMedicine* *51*, 102503. <https://doi.org/10.1016/j.ebiom.2019.10.029>.
- Hazleton, J.E., Berman, J.W., and Eugenin, E.A. (2012). Purinergic receptors are required for HIV-1 infection of primary human macrophages. *J. Immunol.* *188*, 4488–4495. <https://doi.org/10.4049/jimmunol.1102482>.
- Orellana, J.A., Velasquez, S., Williams, D.W., Sáez, J.C., Berman, J.W., and Eugenin, E.A. (2013). Pannexin1 hemichannels are critical for HIV infection of human primary CD4+ T lymphocytes. *J. Leukoc. Biol.* *94*, 399–407. <https://doi.org/10.1189/jlb.0512249>.
- Hernandez, C.A., and Eliseo, E. (2022). The Role of Pannexin-1 Channels in HIV and NeuroHIV Pathogenesis. *Cells* *11*. <https://doi.org/10.3390/cells11142245>.
- Gorska, A.M., Donoso, M., Valdebenito, S., Prideaux, B., Queen, S., Scemes, E., Clements, J., and Eugenin, E. (2021). Human immunodeficiency virus-1/simian immunodeficiency virus infection induces opening of pannexin-1 channels resulting in neuronal synaptic compromise: A novel therapeutic opportunity to prevent NeuroHIV. *J. Neurochem.* *158*, 500–521. <https://doi.org/10.1111/jnc.15374>.
- Gordon, J.L. (1986). Extracellular ATP: effects, sources and fate. *Biochem. J.* *233*, 309–319. <https://doi.org/10.1042/bj2330309>.
- Lévesque, S.A., Kukulski, F., Enjyoji, K., Robson, S.C., and Sévigny, J. (2010). NTPDase1 governs P2X7-dependent functions in murine macrophages. *Eur. J. Immunol.* *40*, 1473–1485. <https://doi.org/10.1002/eji.200939741>.
- Muller, W.A. (2011). Mechanisms of leukocyte transendothelial migration. *Annu. Rev. Pathol.* *6*, 323–344. <https://doi.org/10.1146/annurev-pathol-011110-130224>.
- Feng, D., Nagy, J.A., Pyne, K., Dvorak, H.F., and Dvorak, A.M. (1998). Neutrophils emigrate from venules by a transendothelial cell pathway in response to FMLP. *J. Exp. Med.* *187*, 903–915. <https://doi.org/10.1084/jem.187.6.903>.

16. Granger, D.N., and Senchenkova, E. (2010). Inflammation and the Microcirculation, p. NBK53373.
17. Eugenin, E.A., Osiecki, K., Lopez, L., Goldstein, H., Calderon, T.M., and Berman, J.W. (2006). CCL2/monocyte chemoattractant protein-1 mediates enhanced transmigration of human immunodeficiency virus (HIV)-infected leukocytes across the blood-brain barrier: a potential mechanism of HIV-CNS invasion and NeuroAIDS. *J. Neurosci.* 26, 1098–1106. <https://doi.org/10.1523/JNEUROSCI.3863-05.2006>.
18. Veenstra, M., León-Rivera, R., Li, M., Gama, L., Clements, J.E., and Berman, J.W. (2017). Mechanisms of CNS Viral Seeding by HIV. *mBio* 8, e01280-17. <https://doi.org/10.1128/mBio.01280-17>.
19. Williams, D.W., Anastos, K., Morgello, S., and Berman, J.W. (2015). JAM-A and ALCAM are therapeutic targets to inhibit diapedesis across the BBB of CD14+CD16+ monocytes in HIV-infected individuals. *J. Leukoc. Biol.* 97, 401–412. <https://doi.org/10.1189/jlb.5A0714-347R>.
20. Carman, C.V., Sage, P.T., Sciuto, T.E., de la Fuente, M.A., Geha, R.S., Ochs, H.D., Dvorak, H.F., Dvorak, A.M., and Springer, T.A. (2007). Transcellular diapedesis is initiated by invasive podosomes. *Immunity* 26, 784–797. <https://doi.org/10.1016/j.immuni.2007.04.015>.
21. Jacob, F., Pérez Novo, C., Bachert, C., and Van Crombruggen, K. (2013). Purinergic signaling in inflammatory cells: P2 receptor expression, functional effects, and modulation of inflammatory responses. *Purinergic Signal.* 9, 285–306. <https://doi.org/10.1007/s11302-013-9357-4>.
22. Knowles, J.R. (1980). Enzyme-catalyzed phosphoryl transfer reactions. *Annu. Rev. Biochem.* 49, 877–919. <https://doi.org/10.1146/annurev.bi.49.070180.004305>.
23. Satchell, D.G., and Burnstock, G. (1971). Quantitative studies of the release of purine compounds following stimulation of non-adrenergic inhibitory nerves in the stomach. *Biochem. Pharmacol.* 20, 1694–1697. [https://doi.org/10.1016/0006-2952\(71\)90299-1](https://doi.org/10.1016/0006-2952(71)90299-1).
24. Müller, C.E., Baqi, Y., and Namasivayam, V. (2020). Agonists and Antagonists for Purinergic Receptors. *Methods Mol. Biol.* 2041, 45–64. [https://doi.org/10.1007/978-1-4939-9717-6\\_3](https://doi.org/10.1007/978-1-4939-9717-6_3).
25. Daneman, R., and Prat, A. (2015). The blood-brain barrier. *Cold Spring Harb. Perspect. Biol.* 7, a020412. <https://doi.org/10.1101/cshperspect.a020412>.
26. Veenstra, M., Byrd, D.A., Inglese, M., Buyukturkoglu, K., Williams, D.W., Fleysher, L., Li, M., Gama, L., León-Rivera, R., Calderon, T.M., et al. (2019). CCR2 on Peripheral Blood CD14. *J. Neuroimmune Pharmacol.* 14, 120–133. <https://doi.org/10.1007/s11481-018-9792-7>.
27. Zhao, Y., Gan, L., Ren, L., Lin, Y., Ma, C., and Lin, X. (2022). Factors influencing the blood-brain barrier permeability. *Brain Res.* 1788, 147937. <https://doi.org/10.1016/j.brainres.2022.147937>.
28. Eugenin, E.A., Gamss, R., Buckner, C., Buono, D., Klein, R.S., Schoenbaum, E.E., Calderon, T.M., and Berman, J.W. (2006). Shedding of PECAM-1 during HIV infection: a potential role for soluble PECAM-1 in the pathogenesis of NeuroAIDS. *J. Leukoc. Biol.* 79, 444–452. <https://doi.org/10.1189/jlb.0405215>.
29. Vestweber, D. (2008). VE-cadherin: the major endothelial adhesion molecule controlling cellular junctions and blood vessel formation. *Arterioscler. Thromb. Vasc. Biol.* 28, 223–232. <https://doi.org/10.1161/ATVBAHA.107.158014>.
30. Hunt, P.W., Martin, J.N., Sinclair, E., Bredt, B., Hagos, E., Lampiris, H., and Deeks, S.G. (2003). T cell activation is associated with lower CD4+ T cell gains in human immunodeficiency virus-infected patients with sustained viral suppression during antiretroviral therapy. *J. Infect. Dis.* 187, 1534–1543. <https://doi.org/10.1086/374786>.
31. Gendelman, H.E., Orenstein, J.M., Martin, M.A., Ferrua, C., Mitra, R., Phipps, T., Wahl, L.A., Lane, H.C., Fauci, A.S., and Burke, D.S. (1988). Efficient isolation and propagation of human immunodeficiency virus on recombinant colony-stimulating factor 1-treated monocytes. *J. Exp. Med.* 167, 1428–1441. <https://doi.org/10.1084/jem.167.4.1428>.
32. Westervelt, P., Gendelman, H.E., and Ratner, L. (1991). Identification of a determinant within the human immunodeficiency virus 1 surface envelope glycoprotein critical for productive infection of primary monocytes. *Proc. Natl. Acad. Sci. USA* 88, 3097–3101. <https://doi.org/10.1073/pnas.88.8.3097>.
33. Gendelman, H.E., Baca, L.M., Kubrak, C.A., Genis, P., Burrous, S., Friedman, R.M., Jacobs, D., and Meltzer, M.S. (1992). Induction of IFN- $\alpha$  in peripheral blood mononuclear cells by HIV-infected monocytes. Restricted antiviral activity of the HIV-induced IFN. *J. Immunol.* 148, 422–429.
34. Gendelman, H.E., Orenstein, J.M., Baca, L.M., Weiser, B., Burger, H., Kalter, D.C., and Meltzer, M.S. (1989). The macrophage in the persistence and pathogenesis of HIV infection. *AIDS* 3, 475–495. <https://doi.org/10.1097/00002030-198908000-00001>.
35. Freed, E.O., Englund, G., and Martin, M.A. (1995). Role of the basic domain of human immunodeficiency virus type 1 matrix in macrophage infection. *J. Virol.* 69, 3949–3954. <https://doi.org/10.1128/JVI.69.6.3949-3954.1995>.
36. Mishra, Y.G., and Manavathi, B. (2021). Focal adhesion dynamics in cellular function and disease. *Cell. Signal.* 85, 110046. <https://doi.org/10.1016/j.cellsig.2021.110046>.
37. Kalsi, K., Lawson, C., Dominguez, M., Taylor, P., Yacoub, M.H., and Smolenski, R.T. (2002). Regulation of ecto-5'-nucleotidase by TNF- $\alpha$  in human endothelial cells. *Mol. Cell. Biochem.* 232, 113–119. <https://doi.org/10.1023/a:1014806916844>.
38. Strain, J.F., Burdo, T.H., Song, S.K., Sun, P., El-Ghazzawy, O., Nelson, B., Westerhaus, E., Baker, L., Vaida, F., and Ances, B.M. (2017). Diffusion Basis Spectral Imaging Detects Ongoing Brain Inflammation in Virologically Well-Controlled HIV+ Patients. *J. Acquir. Immune Defic. Syndr.* 76, 423–430. <https://doi.org/10.1097/QAI.0000000000001513>.
39. Mina, Y., Wu, T., Hsieh, H.C., Hammoud, D.A., Shah, S., Lau, C.Y., Ham, L., Snow, J., Horne, E., Ganesan, A., et al. (2021). Association of White Matter Hyperintensities With HIV Status and Vascular Risk Factors. *Neurology* 96, e1823–e1834. <https://doi.org/10.1212/WNL.0000000000001702>.
40. Kelder, W., McArthur, J.C., Nance-Sproson, T., McClernon, D., and Griffin, D.E. (1998). Beta-chemokines MCP-1 and RANTES are selectively increased in cerebrospinal fluid of patients with human immunodeficiency virus-associated dementia. *Ann. Neurol.* 44, 831–835. <https://doi.org/10.1002/ana.410440521>.
41. Ansari, A.W., Bhatnagar, N., Dittrich-Breiholz, O., Kracht, M., Schmidt, R.E., and Heiken, H. (2006). Host chemokine (C-C motif) ligand-2 (CCL2) is differentially regulated in HIV type 1 (HIV-1)-infected individuals. *Int. Immunol.* 18, 1443–1451. <https://doi.org/10.1093/intimm/dxl078>.
42. Seiffert, K., Ding, W., Wagner, J.A., and Granstein, R.D. (2006). ATP $\gamma$ S enhances the production of inflammatory mediators by a human dermal endothelial cell line via purinergic receptor signaling. *J. Invest. Dermatol.* 126, 1017–1027. <https://doi.org/10.1038/sj.jid.5700135>.
43. Tibbetts, S.A., Seetharama Jois, D., Siahaan, T.J., Benedict, S.H., and Chan, M.A. (2000). Linear and cyclic LFA-1 and ICAM-1 peptides inhibit T cell adhesion and function. *Peptides* 21, 1161–1167. [https://doi.org/10.1016/s0196-9781\(00\)00255-2](https://doi.org/10.1016/s0196-9781(00)00255-2).
44. Muller, W.A. (2016). Transendothelial migration: unifying principles from the endothelial perspective. *Immunol. Rev.* 273, 61–75. <https://doi.org/10.1111/imr.12443>.
45. Sperber, H.S., Raymond, K.A., Bouzidi, M.S., Ma, T., Valdebenito, S., Eugenin, E., Roan, N.R., Deeks, S.G., Winning, S., Fandrey, J., et al. (2023). The Hypoxia-Regulated Ectonucleotidase CD73 Is a Host Determinant of HIV Latency.
46. Chekeni, F.B., Elliott, M.R., Sandilos, J.K., Walk, S.F., Kinchen, J.M., Lazarowski, E.R., Armstrong, A.J., Penuela, S., Laird, D.W., Salvendy, G.S., et al. (2010). Pannexin 1 channels mediate 'find-me' signal release and membrane permeability during apoptosis. *Nature* 467, 863–867. <https://doi.org/10.1038/nature09413>.
47. Elliott, M.R., Chekeni, F.B., Trampont, P.C., Lazarowski, E.R., Kadl, A., Walk, S.F., Park, D., Woodson, R.I., Ostankovich, M., Sharma, P., et al. (2009). Nucleotides released by apoptotic cells act as a find-me signal to promote phagocytic clearance. *Nature* 461, 282–286. <https://doi.org/10.1038/nature08296>.
48. Shoji, K.F., Sáez, P.J., Harcha, P.A., Aguila, H.L., and Sáez, J.C. (2014). Pannexin1 channels act downstream of P2X 7 receptors in ATP-induced murine T-cell death. *Channels* 8, 142–156. <https://doi.org/10.4161/chan.28122>.
49. Di Virgilio, F., Sarti, A.C., and Coutinho-Silva, R. (2020). Purinergic signaling, DAMPs, and inflammation. *Am. J. Physiol. Cell Physiol.* 318, C832–C835. <https://doi.org/10.1152/ajpcell.00053.2020>.
50. Tripathy, A., Padhan, P., Swain, N., Raghav, S.K., and Gupta, B. (2021). Increased Extracellular ATP in Plasma of Rheumatoid Arthritis Patients Activates CD8. *Arch. Med. Res.* 52, 423–433. <https://doi.org/10.1016/j.arcmed.2020.12.010>.
51. Stachon, P., Geis, S., Peikert, A., Heidenreich, A., Michel, N.A., Ünal, F., Hoppe, N., Dufner, B., Schulte, L., Marchini, T., et al. (2016). Extracellular ATP Induces Vascular Inflammation and Atherosclerosis via Purinergic Receptor Y2 in Mice. *Arterioscler. Thromb. Vasc. Biol.* 36, 1577–1586. <https://doi.org/10.1161/ATVBAHA.115.307397>.
52. Luu, R., Valdebenito, S., Scemes, E., Cibelli, A., Spray, D.C., Rovegno, M., Tichauer, J., Cottignies-Calamarte, A., Rosenberg, A., Capron, C., et al. (2021). Pannexin-1 channel opening is critical for COVID-19

- pathogenesis. *iScience* 24, 103478. <https://doi.org/10.1016/j.isci.2021.103478>.
53. Linden, J., Koch-Nolte, F., and Dahl, G. (2019). Purine Release, Metabolism, and Signaling in the Inflammatory Response. *Annu. Rev. Immunol.* 37, 325–347. <https://doi.org/10.1146/annurev-immunol-051116-052406>.
  54. Eltzschig, H.K., Sitkovsky, M.V., and Robson, S.C. (2012). Purinergic signaling during inflammation. *N. Engl. J. Med.* 367, 2322–2333. <https://doi.org/10.1056/NEJMr1205750>.
  55. Henttinen, T., Jaikonen, S., and Yegutkin, G.G. (2003). Adherent leukocytes prevent adenosine formation and impair endothelial barrier function by Ecto-5'-nucleotidase/CD73-dependent mechanism. *J. Biol. Chem.* 278, 24888–24895. <https://doi.org/10.1074/jbc.M300779200>.
  56. Malik, S., Valdebenito, S., D'Amico, D., Prideaux, B., and Eugenin, E.A. (2021). HIV infection of astrocytes compromises inter-organellar interactions and inositol phosphate metabolism: A potential mechanism of bystander damage and viral reservoir survival. *Prog. Neurobiol.* 206, 102157. <https://doi.org/10.1016/j.pneurobio.2021.102157>.
  57. Martin, M.W., and Harden, T.K. (1989). Agonist-induced desensitization of a P2Y-purinergic receptor-regulated phospholipase C. *J. Biol. Chem.* 264, 19535–19539.
  58. Coddou, C., Yan, Z., and Stojilkovic, S.S. (2015). Role of domain calcium in purinergic P2X2 receptor channel desensitization. *Am. J. Physiol. Cell Physiol.* 308, C729–C736. <https://doi.org/10.1152/ajpcell.00399.2014>.
  59. Merighi, S., Poloni, T.E., Terrazzan, A., Moretti, E., Gessi, S., and Ferrari, D. (2021). Alzheimer and Purinergic Signaling: Just a Matter of Inflammation? *Cells* 10. <https://doi.org/10.3390/cells10051267>.
  60. Burnstock, G. (2017). Purinergic Signaling in the Cardiovascular System. *Circ. Res.* 120, 207–228. <https://doi.org/10.1161/CIRCRESAHA.116.309726>.
  61. Eberhardt, N., Bergero, G., Mazzocco Mariotta, Y.L., and Aoki, M.P. (2022). Purinergic modulation of the immune response to infections. *Purinergic Signal.* 18, 93–113. <https://doi.org/10.1007/s11302-021-09838-y>.
  62. Guns, P.J.D.F., Hendrickx, J., Van Assche, T., Fransen, P., and Bult, H. (2010). P2Y receptors and atherosclerosis in apolipoprotein E-deficient mice. *Br. J. Pharmacol.* 159, 326–336. <https://doi.org/10.1111/j.1476-5381.2009.00497.x>.
  63. Cochain, C., and Zerneck, A. (2016). CD39 identifies a microenvironment-specific anti-inflammatory CD8+ T-cell population in atherosclerotic lesions. *Basic Res. Cardiol.* 111, 71. <https://doi.org/10.1007/s00395-016-0589-7>.
  64. Dorsam, R.T., and Kunapuli, S.P. (2004). Central role of the P2Y12 receptor in platelet activation. *J. Clin. Invest.* 113, 340–345. <https://doi.org/10.1172/JCI20986>.
  65. Johnston, L.R., La Flamme, A.C., Larsen, P.D., and Harding, S.A. (2015). Prasugrel inhibits platelet-enhanced pro-inflammatory CD4+ T cell responses in humans. *Atherosclerosis* 239, 283–286. <https://doi.org/10.1016/j.atherosclerosis.2015.01.006>.
  66. van Duijn, J., van Elsas, M., Benne, N., Depuydt, M., Wezel, A., Smeets, H., Bot, I., Jiskoot, W., Kuiper, J., and Slütter, B. (2019). CD39 identifies a microenvironment-specific anti-inflammatory CD8+ T-cell population in atherosclerotic lesion. *Atherosclerosis* 285, 71–78. <https://doi.org/10.1016/j.atherosclerosis.2019.04.217>.
  67. Dai, X.P., Wu, F.Y., Cui, C., Liao, X.J., Jiao, Y.M., Zhang, C., Song, J.W., Fan, X., Zhang, J.Y., He, Q., and Wang, F.S. (2021). Increased Platelet-CD4+ T Cell Aggregates Are Correlated With HIV-1 Permissiveness and CD4+ T Cell Loss. *Front. Immunol.* 12, 799124. <https://doi.org/10.3389/fimmu.2021.799124>.
  68. Seye, C.I., Yu, N., Jain, R., Kong, Q., Minor, T., Newton, J., Erb, L., González, F.A., and Weisman, G.A. (2003). The P2Y2 nucleotide receptor mediates UTP-induced vascular cell adhesion molecule-1 expression in coronary artery endothelial cells. *J. Biol. Chem.* 278, 24960–24965. <https://doi.org/10.1074/jbc.M301439200>.
  69. Bogle, R.G., Coade, S.B., Moncada, S., Pearson, J.D., and Mann, G.E. (1991). Bradykinin and ATP stimulate L-arginine uptake and nitric oxide release in vascular endothelial cells. *Biochem. Biophys. Res. Commun.* 180, 926–932. [https://doi.org/10.1016/s0006-291x\(05\)81154-4](https://doi.org/10.1016/s0006-291x(05)81154-4).
  70. Van Coevorden, A., and Boeynaems, J.M. (1984). Physiological concentrations of ADP stimulate the release of prostacyclin from bovine aortic endothelial cells. *Prostaglandins* 27, 615–626. [https://doi.org/10.1016/0090-6980\(84\)90097-2](https://doi.org/10.1016/0090-6980(84)90097-2).
  71. D'Amico, D., Barone, R., Di Felice, V., Ances, B., Prideaux, B., and Eugenin, E.A. (2023). Chronic brain damage in HIV-infected individuals under antiretroviral therapy is associated with viral reservoirs, sulfatide release, and compromised cell-to-cell communication. *Cell. Mol. Life Sci.* 80, 116. <https://doi.org/10.1007/s00018-023-04757-0>.
  72. Bose, S., and Cho, J. (2013). Role of chemokine CCL2 and its receptor CCR2 in neurodegenerative diseases. *Arch. Pharm. Res. (Seoul)* 36, 1039–1050. <https://doi.org/10.1007/s12272-013-0161-z>.
  73. McLaurin, K.A., Booze, R.M., and Mactutus, C.F. (2019). Diagnostic and prognostic biomarkers for HAND. *J. Neurovirol.* 25, 686–701. <https://doi.org/10.1007/s13365-018-0705-6>.
  74. Wimmer, I., Tietz, S., Nishihara, H., Deutsch, U., Sallusto, F., Gosselet, F., Lyck, R., Müller, W.A., Lassmann, H., and Engelhardt, B. (2019). PECAM-1 Stabilizes Blood-Brain Barrier Integrity and Favors Paracellular T-Cell Diapedesis Across the Blood-Brain Barrier During Neuroinflammation. *Front. Immunol.* 10, 711. <https://doi.org/10.3389/fimmu.2019.00711>.
  75. Jaczewska, J., Abdulreda, M.H., Yau, C.Y., Schmitt, M.M., Schubert, I., Berggren, P.O., Weber, C., Koenen, R.R., Moy, V.T., and Wojcikiewicz, E.P. (2014). TNF- $\alpha$  and IFN- $\gamma$  promote lymphocyte adhesion to endothelial junctional regions facilitating transendothelial migration. *J. Leukoc. Biol.* 95, 265–274. <https://doi.org/10.1189/jlb.0412205>.
  76. Stamatovic, S.M., Sladojevic, N., Keep, R.F., and Andjelkovic, A.V. (2012). Relocalization of junctional adhesion molecule A during inflammatory stimulation of brain endothelial cells. *Mol. Cell Biol.* 32, 3414–3427. <https://doi.org/10.1128/MCB.06678-11>.
  77. Millán, J., Cain, R.J., Reglero-Real, N., Bigarella, C., Marcos-Ramiro, B., Fernández-Martin, L., Correas, I., and Ridley, A.J. (2010). Adherens junctions connect stress fibres between adjacent endothelial cells. *BMC Biol.* 8, 11. <https://doi.org/10.1186/1741-7007-8-11>.
  78. Stroka, K.M., Vaitkus, J.A., and Aranda-Espinoza, H. (2012). Endothelial cells undergo morphological, biomechanical, and dynamic changes in response to tumor necrosis factor- $\alpha$ . *Eur. Biophys. J.* 41, 939–947. <https://doi.org/10.1007/s00249-012-0851-3>.
  79. Wang, J., and Chen, X. (2022). Junctional Adhesion Molecules: Potential Proteins in Atherosclerosis. *Front. Cardiovasc. Med.* 9, 888818. <https://doi.org/10.3389/fcvm.2022.888818>.
  80. Lécuyer, M.A., Saint-Laurent, O., Bourbonnière, L., Larouche, S., Larochelle, C., Michel, L., Charabati, M., Abadier, M., Zandee, S., Haghayegh Jahromi, N., et al. (2017). Dual role of ALCAM in neuroinflammation and blood-brain barrier homeostasis. *Proc. Natl. Acad. Sci. USA* 114, E524–E533. <https://doi.org/10.1073/pnas.1614336114>.
  81. Willrodt, A.H., Salabarría, A.C., Schineis, P., Ignatova, D., Hunter, M.C., Vranova, M., Golding-Ochsenbein, A.M., Sigmund, E., Romagna, A., Strassberger, V., et al. (2019). ALCAM Mediates DC Migration Through Afferent Lymphatics and Promotes Allo-specific Immune Reactions. *Front. Immunol.* 10, 759. <https://doi.org/10.3389/fimmu.2019.00759>.
  82. Wu, S.T., Han, J.R., Yao, N., Li, Y.L., Zhang, F., Shi, Y., Shi, F.D., and Li, Z.G. (2022). Activation of P2X4 receptor exacerbates acute brain injury after intracerebral hemorrhage. *CNS Neurosci. Ther.* 28, 1008–1018. <https://doi.org/10.1111/cns.13831>.
  83. Srivastava, P., Cronin, C.G., Scranton, V.L., Jacobson, K.A., Liang, B.T., and Verma, R. (2020). Neuroprotective and neuro-rehabilitative effects of acute purinergic receptor P2X4 (P2X4R) blockade after ischemic stroke. *Exp. Neurol.* 329, 113308. <https://doi.org/10.1016/j.expneurol.2020.113308>.
  84. Sagar, D., Lamontagne, A., Foss, C.A., Khan, Z.K., Pomper, M.G., and Jain, P. (2012). Dendritic cell CNS recruitment correlates with disease severity in EAE via CCL2 chemotaxis at the blood-brain barrier through paracellular transmigration and ERK activation. *J. Neuroinflammation* 9, 245. <https://doi.org/10.1186/1742-2094-9-245>.
  85. Wu, H., Deng, R., Chen, X., Wong, W.C., Chen, H., Gao, L., Nie, Y., Wu, W., and Shen, J. (2016). Caveolin-1 Is Critical for Lymphocyte Trafficking into Central Nervous System during Experimental Autoimmune Encephalomyelitis. *J. Neurosci.* 36, 5193–5199. <https://doi.org/10.1523/JNEUROSCI.3734-15.2016>.
  86. Phillipson, M., and Kubes, P. (2011). The neutrophil in vascular inflammation. *Nat. Med.* 17, 1381–1390. <https://doi.org/10.1038/nm.2514>.
  87. Eugenin, E.A., Clements, J.E., Zink, M.C., and Berman, J.W. (2011). Human immunodeficiency virus infection of human astrocytes disrupts blood-brain barrier integrity by a gap junction-dependent

- mechanism. *J. Neurosci.* 31, 9456–9465. <https://doi.org/10.1523/JNEUROSCI.1460-11.2011>.
88. Eugenin, E.A., and Berman, J.W. (2003). Chemokine-dependent mechanisms of leukocyte trafficking across a model of the blood-brain barrier. *Methods* 29, 351–361. [https://doi.org/10.1016/s1046-2023\(02\)00359-6](https://doi.org/10.1016/s1046-2023(02)00359-6).
89. Lambrecht, G. (2000). Agonists and antagonists acting at P2X receptors: selectivity profiles and functional implications. *Naunyn-Schmiedeberg's Arch. Pharmacol.* 362, 340–350. <https://doi.org/10.1007/s002100000312>.
90. Carman, C.V., and Springer, T.A. (2004). A trans migratory cup in leukocyte diapedesis both through individual vascular endothelial cells and between them. *J. Cell Biol.* 167, 377–388. <https://doi.org/10.1083/jcb.200404129>.
91. Donoso, M., D'Amico, D., Valdebenito, S., Hernandez, C.A., Prideaux, B., and Eugenin, E.A. (2022). Identification, Quantification, and Characterization of HIV-1 Reservoirs in the Human Brain. *Cells* 11. <https://doi.org/10.3390/cells11152379>.

**STAR★METHODS**

**KEY RESOURCES TABLE**

REAGENT or RESOURCE	SOURCE	IDENTIFIER
<i>Antibodies</i>		
CD4	Abcam	Cat# ab133616; RRID:AB_2750883
VE-Cadherin	Santa Cruz	Cat# sc-6458; RRID:AB_2077955
HIV-p24-biotin	Genetex	Cat# GTX40774; RRID:AB_424248
JAM-A	Sigma	Cat# 36-1700; RRID:AB_2533241
JAM-A	Santa Cruz	Cat# sc-53623; RRID:AB_784134
PECAM-1	Santa Cruz	Cat# sc-8306; RRID:AB_653100
CD99	ThermoFisher Scientific	Cat# MA512287; RRID:AB_10979312
CD99	Zymed	Cat# 180235; RRID:AB_86733
ZO-1	ThermoFisher Scientific	Cat# 40-2200; RRID:AB_2533456
Claudin-1	ThermoFisher Scientific	Cat# 51-9000; RRID:AB_87435
Occludin	ThermoFisher Scientific	Cat# SAB4200489
ICAM-1	Sigma	Cat# SAB4300383; RRID:AB_10621182
ICAM-1	ThermoFisher Scientific	Cat# 16-0549-82; RRID:AB_468981
CD11a	ThermoFisher Scientific	Cat# PA5-79531; RRID:AB_2746646
NT5E	Sigma	Cat# SAB5300408
ENTPD-1	Sigma	Cat# SAB4301784
Adenosine deaminase	ThermoFisher Scientific	Cat# PA5-51572; RRID:2637694
CD38	Proteintech	Cat# 25284-1-AP; RRID:AB_2880007
MMP-2	Sigma	Cat# M6302; RRID:AB_260614
Talin	ThermoFisher Scientific	Cat# MA5-28133; RRID:AB_2745116
Paxillin	ThermoFisher Scientific	Cat# AHO0492; RRID:AB_2536312
Vinculin	Abcam	Cat# ab91459; RRID:AB_2050446
FAK	Proteintech	Cat# 12636-1-AP; RRID:AB_2173668
P2X <sub>1</sub>	ThermoFisher Scientific	Cat# PA577662; RRID:AB_2736289
P2X <sub>4</sub>	ThermoFisher Scientific	Cat# PA5-83466; RRID:AB_2790621
P2X <sub>5</sub>	Alomone	Cat# APR005; RRID:AB_2040060
P2X <sub>7</sub>	Sigma	Cat# P8232; RRID:AB_261204
P2Y <sub>1</sub>	ThermoFisher Scientific	Cat# MA5-31815; RRID:AB_2787438
P2Y <sub>2</sub>	ThermoFisher Scientific	Cat# PA1-46150; RRID:AB_2156124
P2Y <sub>6</sub>	Alamone	Cat# APR-011; RRID:AB_2040082
P2Y <sub>11</sub>	Alamone	Cat# APR-015; RRID:AB_2040072
ENTPD-2	ThermoFisher Scientific	Cat# HPA017676; RRID:AB_1848179
ENTPD-3	ThermoFisher Scientific	Cat# PA524209; RRID:AB_2541709
ENTPD-8	ThermoFisher Scientific	Cat# PA5-25085; RRID:AB_2542585
GAPDH	Cell Signaling	Cat# 2118; RRID:AB_561053

(Continued on next page)

**Continued**

REAGENT or RESOURCE	SOURCE	IDENTIFIER
Anti-Rabbit-HRP	Cell Signaling	Cat# 7074; RRID:AB_2099233
Anti-Mouse-HRP	Cell Signaling	Cat# 7076; RRID:AB_330924
Live/Dead Aqua	ThermoFisher Scientific	Cat# L34966
Anti-Rabbit AlexaFluor 594	ThermoFisher Scientific	Cat# A11012; RRID:AB_2534079
Anti-Mouse AlexaFluor 647	ThermoFisher Scientific	Cat# A21235; RRID:AB_2535804
Anti-Goat AlexaFluor 488	ThermoFisher Scientific	Cat# A21206; RRID:AB_2535792
Anti-Rabbit AlexaFluor 568	ThermoFisher Scientific	Cat# A11057; RRID:AB_2534104
Anti-Rabbit AlexaFluor 800	ThermoFisher Scientific	Cat# A32735; RRID:AB_2633284
Anti-Mouse AlexaFluor 800	ThermoFisher Scientific	Cat# A32730; RRID:AB_2633279
Phalloidin AlexaFluor 680	ThermoFisher Scientific	Cat# A22286
Streptavidin Alexa Fluor 647	ThermoFisher Scientific	Cat# S32357
Mouse IgG <sub>1</sub> protein	MP Biomedicals (formerly Cappel)	Cat# MOP21
Goat serum	Sigma	Cat# G9023
Normal Rabbit IgG	Cell Signaling	Cat# 2729

**Biological samples**

BMVEC	Primary cells isolated from the frontal and occipital cortex	N/A
PBMCs, derived from Leukopacks	Gulf Coast Regional Blood Center, Houston, TX	N/A
HIV <sub>ADA</sub> viral isolate	NIH AIDS Reagent Program, Germantown, MD	Cat# ARP-416
pNL(AD <sub>3</sub> ) molecular clone	NIH AIDS Reagent Program, Germantown, MD	Cat# ARP-11346

**Chemicals/Materials**

RPMI	ThermoFisher Scientific	Cat# 11995-065
Fetal bovine serum	ThermoFisher Scientific	Cat# 16000044
PenStrep	ThermoFisher Scientific	Cat#15140-122
0.05% Trypsin EDTA	ThermoFisher Scientific	Cat# 25300-054
Tryp-LE Select	ThermoFisher Scientific	Cat# A1217701
ATP Na <sup>+</sup>	Sigma	Cat# A1852
ATPγS Li <sup>+</sup>	Sigma	Cat# 119120
Phytohemagglutinin (PHA)	Sigma	Cat# AC356150050
Recombinant Human TNFα	R&D Systems	Cat# 210-TA
Paraformaldehyde	Sigma-Aldrich	Cat# P6148
Gelatin (from cold water fish)	Sigma-Aldrich	Cat# G7041
BSA (Bovine serum albumin)	Sigma-Aldrich	Cat# 05470
10X RIPA Buffer	Cell Signaling	Cat# 9806
Horse serum	Sigma-Aldrich	Cat# H0146
Glycine	ThermoFisher Scientific	Cat# BP381
EDTA	Invitrogen	Cat# 15575-020
M199	ThermoFisher Scientific	Cat# 31100-035
Fetal calf serum	ThermoFisher Scientific	Cat# 16140071
Tris-buffered saline	Fisher-Bioreagents	Cat# BP2471-1
Triton x-100	Sigma	Cat# X100
Immedge pen	Vector Laboratories	Cat# H-4000
Glutamax	ThermoFisher Scientific	Cat# 35050-061

(Continued on next page)

**Continued**

REAGENT or RESOURCE	SOURCE	IDENTIFIER
ProLong™ Gold Antifade Mounting with DAPI	ThermoFisher Scientific	Cat# P36931
Human serum	BioIVT	CAT# HUMANSRMP-HI-1
HEPES	ThermoFisher Scientific	Cat# 15630-080
Type A Gelatin	ThermoFisher Scientific	Cat# 68-500
ACK Lysis Buffer	ThermoFisher Scientific	Cat# A10492-01
Ficoll-Paque	Cytiva	Cat# 17144003
ECL Substrate	Perkin Elmer	Cat# NEL104001EA
β-mercaptoethanol	Sigma	Cat# M3148
Glycerol	Sigma	Cat# G33-4
Sodium dodecyl sulfate	Sigma	Cat# L6026
SYBR Green PCR master mix	ThermoFisher Scientific	Cat# 4309155
TRIzol Reagent	ThermoFisher Scientific	Cat# 15596026
0.45 μm nitrocellulose membrane	Cytiva	Cat# 10600002

**ELISA**

HIV-1 p24	XpressBio	Cat# XB-1000
CCL2	R&D Systems	Cat# DCP00

**Peptides**

cLABL (Cyc 1-12, LFA-1 peptide)	Genscript	Cat# Cyclo (1-12)
Scr (scrambled LFA-1 peptide)	Genscript	Cat# Cyclo (1-12) Scrambled

**Software**

NIS-Elements-AR	Nikon	<a href="https://www.microscope.healthcare.nikon.com">https://www.microscope.healthcare.nikon.com</a>
FlowJo	BD	<a href="https://www.flowjo.com/solutions/flowjo">https://www.flowjo.com/solutions/flowjo</a>
Prism	GraphPad	<a href="https://www.graphpad.com/">https://www.graphpad.com/</a>
ImageJ	NIH	<a href="https://imagej.nih.gov/ij/download.html">https://imagej.nih.gov/ij/download.html</a>
Image Studio	Licor	<a href="https://www.licor.com/bio/image-studio/">https://www.licor.com/bio/image-studio/</a>

**RESOURCE AVAILABILITY**

**Lead contact**

Further information and requests for resources and reagents should be directed to and fulfilled upon reasonable request by the Lead contact Eliseo Eugenin ([eleugenin@utmb.edu](mailto:eleugenin@utmb.edu)). This study did not generate databases or unique reagents.

**Materials availability**

We will share any materials upon reasonable request.

**Data and code availability**

All data reported will be shared by the [lead contact](#) upon request. This manuscript does not report an original code. Any additional information or data required to reanalyze the data reported is available upon reasonable request to the [lead contact](#).

**EXPERIMENTAL MODEL AND STUDY PARTICIPANT DETAILS**

**Cell culture**

No cell lines were used in this study. Primary human brain microvascular endothelial cells (BMVEC) were obtained from frontal/occipital uninfected brains. Peripheral blood mononuclear cells (PBMCs) were obtained from the Gulf Coast Blood Center, Houston, TX. All cultures are grown in separate incubators to prevent any cross-contamination. All cultures were tested for mycoplasma contamination using PCR. For IRB approval, all human cells in this study were exempted. The tissue collection protocols were approved by the Albert Einstein College of Medicine, Rutgers University, and the University of Texas Medical Branch Institutional Review Board (Protocol Numbers, Pro20140000794, Pro2012001303, 18-0136, 18-0135, 18-0134 to E.A.E).

## METHOD DETAILS

### BMVEC cell culture

Low passage (<15) primary human brain microvascular endothelial cells (BMVEC) were cultured on gelatin-coated cell culture dishes using complete M199 media (M199C) as previously described.<sup>87</sup> BMVECs were isolated from a human brain, from either the frontal or occipital cortex, as previously described.<sup>88</sup> BMVECs were grown to 90-95% confluency before conducting downstream assays, such as flow cytometry, immunocytochemistry, and Western blotting.

### PBMC culture

Peripheral blood mononuclear cells (PBMCs) were collected from leukopacks obtained from healthy patients using a Ficoll gradient method. All donors analyzed were negative for CMV, HIV, hepatitis B and C, West Nile virus, and syphilis (Gulf Coast Blood Center, Houston, TX). With each Leukopack, PBMCs were cultured in RPMI-based media (containing 5% human serum, 10% fetal bovine serum, 10 mM HEPES, and penicillin/streptomycin) in the presence of 5 µg/mL phytohemagglutinin (PHA) and 10 U/mL IL-2 in siliconized tubes at a density of  $2 \times 10^6$  cells/mL. After two days in PHA and IL-2, cells were spun at 300xg for 10 min, resuspended in fresh media with 10 U/mL IL-2, and infected with HIV-1 (10 ng/mL HIV<sub>ADA</sub> or pNL(AD<sub>8</sub>)) for two hours at 37°C. PBMCs were spun as before, the supernatant was aspirated, and the cell pellet was resuspended in fresh media at the same cell density as above in siliconized tubes. At the terminal time point of the experiments, the media was subjected to HIV-p24 quantification by ELISA.

### Establishment of acute ATP-treated cultures

To mimic the conditions within people living with HIV (PWH), high ATP exposure within the circulation, PBMCs, or BMVECs were exposed to ATPγS (a non-hydrolyzable ATP analog). As extracellular ATP (eATP) is quickly degraded, ATPγS was chosen as the sulfur atom within the gamma phosphate position; it is resistant to ecto-nucleotidases.<sup>89</sup> We selected ATPγS due to the profile of ATP receptors expressed by BMVEC as obtained for qRT-PCR and Western blotting analyses (Figure S1). The concentration of ATPγS was chosen to replicate the concentration of ATP within the serum of healthy patients (1-3 µM), and the high concentration was chosen to mimic the most severe HAND form, HAD (15 µM).<sup>7</sup> BMVEC cultures were either exposed to ATPγS for at least seven passages. PBMCs infected *in vitro* with 10 ng/mL of either HIV<sub>ADA</sub><sup>31-34</sup> or pNL(AD<sub>8</sub>) (a CCR5-tropic molecular clone of NL4-3)<sup>35</sup> and after a single round of replication, about 18-24 hours after infection, ATPγS was added to the cultures for acute treatment of 4-5 days (5-6 days post-infection). For the co-culture assay, PBMCs were maintained in ATPγS for only 4 days before addition to the BMVEC culture.

### HIV-p24 and CCL2 ELISA

At the endpoint of ATPγS treatment, supernatants were taken and stored at -80°C until utilized for further analysis. HIV p24 ELISA (Perkin Elmer) was used per the manufacturer's protocol for viral titer. A sandwich ELISA (R&D Systems) was used per the manufacturer's protocol for CCL2.

### BMVEC and PBMC coculture

BMVECs were cultured to confluency in the presence of ATPγS on gelatin-coated glass coverslips. TNFα (10 ng/mL) was added to the BMVECs and the PBMCs at least eight hours before the co-culture as positive control. Once the coverslips of BMVECs were confluent, the co-culture experiment was started by first spinning down the PBMCs, aspirating the supernatant, counting them, and then diluting them to  $10^6$  cells/mL so identical numbers of PBMCs could be added to the BMVECs ( $5 \times 10^4$  PBMCs per well). The PBMCs were added to each of the wells or an equivalent volume of PBMC media only. They were co-cultured for 30 min or 2 h, as previously calibrated for leukocytes' early transendothelial transmigration (TEM) across the human BBB.<sup>90</sup> At the endpoint, the media was aspirated from each well, and each coverslip was quickly washed with 1X HBSS and then aspirated. 4% PFA was added to each of the wells and was incubated at 4°C in the dark. Before staining, the coverslips were washed twice with 1X PBS. They were then permeabilized for one minute at room temperature with 0.1% triton in 1X PBS. After permeabilization, the coverslips were washed twice in 1X PBS, then were blocked using super blocking solution (SBS - 50 mM EDTA, 1% BSA, 1% horse serum, 5% human serum, 1% gelatin from cold water fish) at 4°C overnight, as previously published.<sup>91</sup> The coverslips were then placed into the primary antibody, using αCD4 (Abcam, Cat. ab133616, 1:100) and αVE-Cadherin (Santa Cruz, Cat. sc-6458, 1:200), or equivalent concentrations of corresponding IgG, suspended in SBS. After overnight incubation at 4°C, the coverslips were washed five times in 1X PBS before the coverslips were placed into a secondary antibody. The coverslips were incubated at room temperature for two hours using αGoat AlexaFluor 488 (Cat. A21206, 1:200) and αRabbit AlexaFluor 594 (Cat. A11057, 1:100). Coverslips were washed twice with 1X PBS, then incubated in phalloidin 680 (Cat. A22286, 1:2000) for 30 minutes at room temperature. After the phalloidin stain, the coverslips were washed five times and then mounted onto glass slides using Prolong Gold with DAPI (Cat. P36931). Images were taken on a Nikon A1 confocal microscope using spectral detection. Due to the resolution required to resolve the differing morphologies and Z-localization, high-resolution confocal microscopy was needed to effectively assess and quantify the leukocytes above and within the endothelial cell monolayer as well as their polarity and "cup" formation around them (see example in Figure S2).

### Criteria and quantification of adhesion and transmigratory phenotypes

Attachment: The leukocyte was apically associated with the primary brain microvascular endothelial cells (BMVECs), vascular endothelial cadherin (VE-cadherin) was not clustered to the leukocyte (eliminating transcellular transmigration), and leukocyte morphology was round per the actin staining, indicating the cell was not in a transmigratory state. Transcellular transmigration: The leukocyte nucleus was at the same plane as the BMVEC nucleus, the leukocyte was not localized to BMVEC-to-BMVEC cell junctions, VE-cadherin was clustered around the leukocyte, and the leukocyte was in an elongated or non-round morphology, indicating it was undergoing transmigration. Paracellular transmigration: similar criteria to transcellular transmigration, but the leukocyte localization was at BMVEC-to-BMVEC cell junctions. Ten (five for TNF $\alpha$ ) distinct regions of interest (ROIs) of confluent BMVECs were examined to count and quantitate attachment, paracellular, and transcellular transmigration of leukocytes. TNF $\alpha$  treatment was used as a positive control for endothelial cell activation, attachment, and paracellular transmigration of leukocytes. Due to high donor-to-donor variability, representative results are shown.

### Co-culture blocking assay

Thirty minutes before the co-culture, 20  $\mu$ g/mL  $\alpha$ JAM-A (Santa Cruz, Cat. sc-53623), 20  $\mu$ g/mL  $\alpha$ CD99 (Cat. MA5-12287), or an equivalent concentration of mouse IgG was added to the BMVEC wells for the neutralization conditions of the co-culture, similar to previously published experiments.<sup>19</sup> Additionally, an ICAM-1-blocking peptide, LFA-1-peptide (referred Cyc 1-12 or LFA-pep), derived from the I domain of LFA, was also employed.<sup>43</sup> LFA-pep, or its scrambled peptide (Genscript), was added to the BMVEC at a concentration of 100  $\mu$ M, 30 minutes before the co-culture. After the incubation, the PBMCs were added in identical numbers to the BMVECs, as described above.

### Western blotting

At 90-95% confluency, BMVECs were washed with 1X PBS and then scraped using a cell scraper using 1X RIPA buffer. PBMCs were treated similarly with 1X PBS before resuspending in 1X RIPA buffer. Whole-cell lysates were sonicated and quantitated using Bradford assay, and similar amounts of protein were run on SDS-PAGE after resuspending in 5X loading buffer (5%  $\beta$ -mercaptoethanol, 0.02% bromophenol blue, 30% glycerol, 10% SDS, 250 mM/pH 6.8 Tris-Cl) to a 1X concentration and boiling at 100°C for three minutes. The samples were run on precast 7.5% or 4-20% polyacrylamide gels (TGX gels, Bio-Rad) at 100 volts until the dye front was at the bottom of the gel. The gels were then transferred to nitrocellulose membranes at 300 mA for 60 min at 4°C. Membranes were blocked using 3% milk powder and 1% bovine serum albumin (BSA, fraction V) in 1X TBS plus 0.1% tween (1X TBST) for two hours at room temperature. After blocking, the membranes were incubated at 4°C overnight in primary antibody, prepared in 1X TBST and 1% BSA. Membranes were washed in 1X TBST five times for at least five minutes before incubation in secondary antibody. The membranes were incubated in a secondary antibody (either using an Alexa Fluor 800 or a horse radish peroxidase-conjugated antibody) for two hours at room temperature. Before developing, membranes were washed once again, as before, then were incubated for one minute in ECL substrate (Cat. NEL104001EA) for horseradish peroxidase secondaries, then were imaged on a Licor (Odyssey XF) imager. After imaging, membranes were subject to mild stripping buffer before blocking once again, as before, and then were subsequently probed for the loading control, using the same protocol as above. Densitometric analysis was conducted on Image Studio or ImageJ. Target band intensity was normalized to the loading control, and then the normalized intensity was calculated relative to the untreated for fold change (FC) in expression relative to the untreated.

### Immunofluorescence

BMVECs were grown on glass coverslips to 90-95% confluency, and the media was aspirated, washed with 1X HBSS, then fixed in 4% paraformaldehyde in 1X PBS. Coverslips were permeabilized in 0.1% triton in 1X PBS for one minute, then washed twice in 1X PBS. Coverslips were blocked overnight at 4°C in SBS before the primary antibody. The coverslips were then placed into the primary antibody, or an equivalent concentration of corresponding IgG, suspended in SBS. After overnight incubation at 4°C, the coverslips were washed five times in 1X PBS before the coverslips were placed into a secondary antibody solution. The coverslips were incubated at room temperature for two hours using corresponding secondary antibodies in SBS. Coverslips were washed twice with 1X PBS, then incubated in phalloidin 680 (Cat. A22286, 1:2000) for 30 min at room temperature. After the phalloidin stain, the coverslips were washed five times and then mounted onto glass slides using Prolong Gold with DAPI (Cat. P36935). Images were taken on a Nikon A1 confocal microscope. All immunofluorescence image analysis was conducted using Nikon NIS-Elements software.

### Immunofluorescence quantitation and analysis

A maximal intensity projection was first cast for each image for a representative 2D image. Using the 2D projection, a full field ROI for PECAM-1/JAM-A intensity was determined using 3-5 images per independent experiment. The mean fluorescent intensity (MFI) at EC junctions was determined by using the profile function of the NIS software that was drawn along the length of an EC junction, with the same 16-pixel thickness for an average across the junction. To determine the threshold for intracellular PECAM-1/JAM-A or HIV-p24, a profile was drawn across the length of a cell – this was used as a cutoff for whether the intensity was lower than the average intracellular signal (see main text and [Figures S3 and S4](#)). The profile length was approximately the same at each junction. Still, to account for the differences in length, the discontinuity index was made, which took the number of pixels along the junction below the threshold, divided by the number of pixels observed.

### Flow cytometry

Flow cytometry analysis was performed on fixed single cells in suspension. After staining with fluorophore-conjugated primary antibodies as described above, cells were washed and resuspended in flow buffer (1 mM EDTA, 1% BSA in PBS). All centrifugation steps were performed at 300g x 5 min. Samples were collected in 5 mL Falcon Round Bottom Polystyrene test tubes (352058; Fisher Scientific). Flow cytometry analyses were conducted using a BD FACS Celesta Cell Analyzer. Studies were carried out using FlowJo™ 10 software (Ashland, OR). Cells were gated from debris and doublets based on forward and side scatter. If pertinent, live/dead cell exclusion was conducted using Live/Dead™ Fixable Aqua (L34966, Thermo Fisher), following the manufacturer's recommendations. At least 10,000 events were collected for downstream analysis.

### QUANTIFICATION AND STATISTICAL ANALYSIS

The figure legends can find information on the statistical tests and the exact values of n (number of experiments). All statistical analyses were performed using GraphPad Prism 10.0 (GraphPad Software Inc.). The statistical tests were chosen according to the following: Wilcoxon matched-paired signed-rank tests and linear regression was used to determine differences in the rate of proliferation of BMVEC.  $p < 0.05$  was considered as the level of statistical significance.